

Runaway stars as progenitors of supernovae and gamma-ray bursts

John J. Eldridge¹*, Norbert Langer^{2,3} & Christopher A. Tout¹

¹*Institute of Astronomy, The Observatories, University of Cambridge, Madingley Road, Cambridge, CB3 0HA*

²*Argelander-Institut für Astronomie, Bonn University, Auf dem Hügel 71, 53121 Bonn, Germany*

³*Astronomical Institute, University of Utrecht, Postbus 80000, 3508 TA Utrecht, The Netherlands*

18 October 2021

ABSTRACT

When a core collapse supernova occurs in a binary system, the surviving star as well as the compact remnant emerging from the supernova, may reach a substantial space velocity. With binary population synthesis modelling at solar and one fifth of solar metallicity, we predict the velocities of such runaway stars or binaries. We compile predictions for runaway OB stars, red supergiants and Wolf-Rayet stars, either isolated or with a compact companion. For those stars or binaries which undergo a second stellar explosion we compute their further evolution and the distance travelled until a Type II or Type Ibc supernova or a long or short gamma-ray burst occurs. We find our predicted population of OB runaway stars broadly matches the observed population of stars but, to match the fastest observed Wolf-Rayet runaway stars, we require that black holes receive an asymmetric kick upon formation. We find that at solar metallicity Type Ic supernova progenitors travel shorter distances than the progenitors of other supernova types because they are typically more massive and thus have shorter lifetimes. Those of Type IIP supernovae can fly farthest about 48 pc *on average* at solar metallicity, with about 8 per cent of them reaching 100 pc. In considering the consequences of assuming that the progenitors of long gamma-ray bursts are spun-up secondary stars that experience quasi-homogeneous evolution, we find that such evolution has a dramatic effect on the population of runaway Wolf-Rayet stars and that some 30 per cent of GRBs could occur a hundred parsecs or more from their initial positions. We also consider mergers of double compact object binaries consisting of neutron stars and/or black holes. We find the most common type of visible mergers are neutron star–black hole mergers that are roughly ten times more common than neutron star–neutron star mergers. All compact mergers have a wide range of merger times from years to Gyrs and are predicted to occur three hundred times less often than supernovae in the Milky Way. We also find that there may be a population of low-velocity neutron stars that are ejected from a binary rather than by their own natal kick. These neutrons stars need to be included when the distribution of neutron star kicks is deduced from observations.

Key words: gamma-rays: bursts – binaries: general – supernovae: general – stars: evolution – stars: Wolf-Rayet – stars: general

1 INTRODUCTION

Runaway stars are isolated stars or binaries which have escaped from their parent clusters. A satisfactory set of observational characteristics that defines them is difficult to find. Often, it is assumed that a runaway star must have a space velocity of 30 km s^{-1}

or greater. The most commonly observed massive runaway stars are OB runaways (Blaauw 1961; Gies 1987; Stone 1991; Hoogerwerf, de Bruijne & de Zeeuw 2001; de Wit et al. 2005). Currently about 56 such stars are known in the Galaxy, (Hoogerwerf, de Bruijne & de Zeeuw 2001) with velocities up to 200 km s^{-1} . There are some cases known with velocities greater than 500 km s^{-1} (Heber et al. 2008). These high velocities and the stellar lifetimes of a few million years imply that such stars travel many parsecs from their

* E-mail: jje@ast.cam.ac.uk

initial positions before themselves exploding in core-collapse supernovae (SNe).

There are two scenarios that create massive runaway stars. The first is dynamical ejection scenario (DES) where stars are ejected by close encounters in a dense cluster. The second is the binary supernova scenario (BSS) when one of the stars in a binary under goes a SN explosion and the system becomes unbound. The companion star then travels at roughly its pre-SN orbital velocity. It is thought that both scenarios contribute similar numbers of runaway stars. However evidence suggests that the BSS could be responsible for up to two thirds of observed runaways (Hoogerwerf, de Bruijne & de Zeeuw 2001). Methods to discriminate between the two rely on the observational characteristics of the runaway star. Typically BSS runaways are expected to have a surface compositions that indicates they have experienced a binary interaction, while typical DES runaways might have main-sequence composition. A further complication is that some runaway stars, especially those with velocities in excess of about 200 km s^{-1} , may come from a binary that was ejected by the DES with one star being boosted to high velocities after a BSS ejection as discussed by Pflamm-Altenburg & Kroupa (2010). Such binaries would be less common but could naturally explain the highest velocities observed for runaway stars.

Interest in the final fate of runaway stars has increased owing to the observations of Hammer et al. (2006). They observed that some long gamma-ray bursts (Woosley & Bloom 2006) occur a few hundred parsecs away from the nearest star forming region. Cantiello et al. (2007) suggest that this can be explained if the progenitor of the GRB was the secondary in a binary system that was ejected via the BSS.

Concurrently the observations made by Fruchter et al. (2006), Kelly, Kirshner & Pahre (2008) and Anderson & James (2008) also reveal details of how SNe are distributed in their host galaxies. They found that type Ic SNe and GRBs tend to be associated with the most luminous parts, and thus the sites of most intense star-formation, of galaxies while type II and type Ib SNe tend to be more evenly distributed throughout their host galaxies. Larsson et al. (2007) and Raskin et al. (2008) put this down to the difference in progenitor mass for the different SN types. The most massive stars explode earliest and thus closest to the sites of active star formation. While less massive stars have longer lifetimes and are not as closely associated with the most recent star formation. They did not consider the effect of runaway stars. It is important to understand how runaways change the distribution of SNe within a galaxy to remove any systematic error in determining the nature of different SN progenitors.

In this paper we concern ourselves with describing the population of runaway stars from the BSS and their effect on the distribution of SNe within a galaxy. First we describe our method of simulating the runaways. Secondly we give our predictions for the space velocities of runaway stars, binaries and compact remnants and the distances our model runaways travel before exploding as SNe. Thirdly we outline how this affects how SNe are distributed with respect to their initial locations. Fourthly we perform a similar analysis for the merger of double compact object binaries owing to orbital decay by gravitational radiation. Finally we discuss our results and outline our conclusions.

2 COMPUTATIONAL METHOD

Our method is built upon the models and the population synthesis code described by Eldridge, Izzard & Tout (2008). We use the large number of detailed stellar evolution models that were calculated with the Cambridge STARS evolution code, created by Eggleton (1971) and updated by various authors since (Pols et al. 1995; Eldridge & Tout 2004a; Eldridge, Izzard & Tout 2008). The population synthesis code then uses our detailed binary models to estimate various details of a binary population that are of interest and comparable with observations. For example, the relative numbers of different stellar types, the relative rates of different SN types and, here, the expected velocities of runaway stars. Similar studies have used binary population synthesis to predict the runaway population before (van Rensbergen, Vanbeveren & de Loore 1996; de Donder, Vanbeveren & van Bever 1997; Vanbeveren, van Rensbergen & De Loore 1998; Dray et al. 2005). However this is the first time the effect of runaway stars on the distribution of SNe within galaxies has been considered.

While a full description of our detailed models can be found in Eldridge, Izzard & Tout (2008) we provide a brief overview. All the models employ our standard mass-loss prescription because it agrees best with various observations (Eldridge & Tout 2004b; Eldridge, Izzard & Tout 2008). For pre-WR mass loss, we use the rates of de Jager, Nieuwenhuijzen & van der Hucht (1988) except for OB stars for which we use the theoretical rates of Vink, de Koter & Lamers (2001). When the star becomes a WR star [$X_{\text{surface}} < 0.4$, $\log(T_{\text{eff}}/\text{K}) > 4.0$], we use the rates of Nugis & Lamers (2000). We scale all rates with the standard factor $(Z/Z_{\odot})^{0.5}$ (Kudritzki, Pauldrach & Puls 1987; Heger et al. 2003), except for the rates of Vink, de Koter & Lamers (2001) which include their own metallicity scaling.

We have modified our stellar evolution code to model binary evolution. The details of our binary interaction algorithm are relatively simple compared to the scheme outlined by Hurley, Tout & Pols (2002). We used their scheme as a basis but we changed some details which cannot be directly applied to our detailed stellar evolution calculation. We also make a number of assumptions to keep our code relatively simple. Our aim was to investigate the effect of enhanced mass loss due to binary interactions on stellar lifetimes and populations. Therefore, we concentrated on this rather than every possible physical process which would add more uncertainty to our model. We also make assumptions in calculating our synthetic population to avoid calculating a large number of models. For example, we do not model the accretion on to the secondary in the detailed code. We take the final mass of the secondary at the end of the primary evolution as the initial mass of the secondary when we create our detailed secondary model. This avoids calculating 10 times more secondary models than primary models.

We always define the primary as the initially more massive star and we only evolve one star at a time with our detailed code. When we evolve the primary in detail, it has a shorter evolutionary time-scale than the secondary which remains on the main sequence until after the primary completes its evolution and so we can determine the state of

the secondary with the single stellar evolution equations of Hurley, Pols & Tout (2000). When we evolve the secondary in detail, we assume that its companion is the compact remnant of the primary (a white dwarf, neutron star or black hole) and treat this as a point mass.

If Roche lobe overflow occurs mass lost from the primary is transferred to the secondary but not all is necessarily accreted. Accretion causes the star to expand owing to increased total mass and therefore an increased energy production rate if $\dot{M}_2 \geq M_2/\tau_{\text{KH}}$, where τ_{KH} is the thermal, or Kelvin-Helmholtz, time-scale. We assume that the star's maximum accretion rate is determined by its current mass and its thermal timescale. We define a maximum accretion rate for a star such that $\dot{M}_{2,\text{max}} = M_2/\tau_{\text{KH}}$. If the accretion rate is greater than this, then any additional mass and its orbital angular momentum are lost from the system. In general, stars with lower masses have longer thermal time-scales than more massive stars. Efficient transfer is only possible if the two stars are of nearly equal mass so the thermal time-scales are similar. This is an approximate treatment but provides a similar result to the more complex model of Petrovic, Langer & van der Hucht (2005) who included rotation and found that it led to inefficient mass transfer. For compact companions, we derive the maximum accretion rate from the Eddington limit (Cameron & Mock 1967).

In summary our stellar models are a set of around 15,000 detailed stellar evolution models of single stars, primary stars, secondary stars and merged systems (Eldridge, Izzard & Tout 2008). We also include a new series of models to account for quasi-homogeneous evolution. These are discussed below. For this work we made several refinements to our population synthesis code to predict runaway velocities and account for the possibility of SN reversal. That is when the initially lower-mass secondary star undergoes its SN first after mass accretion.

2.1 Population synthesis

Our population synthesis calculations are built upon those described by Eldridge, Izzard & Tout (2008) with some improvements. Here we focus on the evolution after the first SN in the binary. First we estimate the lifetimes of the primary and the secondary star. Our secondary models only have a limited companion mass range but this provides a reasonable estimate because the lifetime varies little with different amounts of mass loss. We compare the lifetimes of the two stars to check whether the SN order is reversed. We find that it is more likely at higher metallicity but only occasional, occurring in 7 per cent of our binary systems. If the secondary lifetime is shorter than the primary lifetime we perform a similar calculation as described below but now the secondary explodes first and may eject the primary star. This gives rise to more stripped SNe occurring away from their initial position.

If a star has a carbon/oxygen core mass greater than $1.38M_{\odot}$ and the final mass of the star is greater than $2M_{\odot}$ we assume it explodes in a SN. We select the SN type as described below. We estimate what type of compact remnant a stellar model will produce by using the method outline in Eldridge & Tout (2004b). We assume that first a neutron star is formed at the centre of the star after core collapse of mass $M_{\text{Ch}} = 1.4M_{\odot}$. This produces about 10^{46}J

of energy from the release of gravitational binding energy in neutron star formation. We then assume a hundredth of this energy is transferred into the envelope by some unknown mechanism. The current suggestion is the transfer occurs via neutrinos released from forming the protoneutron star that are thermalized within the envelope or dense outer parts of the core. We integrate the binding energy of the star from the surface towards the centre until we reach 10^{44}J . The envelope outside this region is ejected with the remaining amount forming the remnant. If we have $M_{\text{rem}} > 3M_{\odot}$, it is a black hole and we set $M_{\text{BH}} = M_{\text{rem}}$. Otherwise we have a neutron star with mass $1.4M_{\odot}$. We determine the fate of the binary if a neutron star is formed by the work of Tauris & Takens (1998) and Tauris et al. (1999) with the latest determination for the kick velocity distribution from observations of Hobbs et al. (2005). If the system is unbound then the velocities of both stars are calculated by the method of Tauris & Takens (1998) that considers every relevant factor. However we neglect the supernova impact on the companion star. If the system remains bound then the velocity of both components is the resultant system velocity (Brandt, Podsiadlowski & Sigurdsson 1995). If the remnant is a black hole, we assume that it receives a similar kick. Because the masses of black holes are greater than those of neutron stars we use the kick distribution of Hobbs et al. (2005) but as a momentum distribution. We calculated the black hole kick velocity, v_{BH} from $v_{\text{BH}} = v_{\text{NS}}(1.4M_{\odot}/M_{\text{BH}})$. Where v_{NS} is a kick velocity selected at random from the neutron star kick velocity distribution and M_{BH} is the mass of the black hole. Black holes are not normally considered to have significant kicks although their importance has been investigated by others (Brandt, Podsiadlowski & Sigurdsson 1995; Kalogera 1999; Mirabel et al. 2002, 2004; Voss & Tauris 2003). We find that we must include them or we obtain no runaway WR stars with initial masses greater than $30M_{\odot}$.

The resulting velocities of runaway stars and runaway binaries are recorded. We also record the SN type and its location at the initial position of the binary. We weight each event by a Salpeter IMF and assume the distributions of initial mass ratios and the logarithm of separations are flat. Our models have initial separations that take values between $1 \leq \log_{10}(a/R_{\odot}) \leq 4$ in steps of 0.25 dex. The mass ratio takes values of $q = 0.3, 0.5, 0.7$ and 0.9 . We do not use the $q = 0.1$ models employed by Eldridge, Izzard & Tout (2008) because there is growing evidence that the mass ratio is skewed to larger values in massive binaries (Garmany et al. 1980; Pinsonneault & Stanek 2006; Kobulnicky & Fryer 2007; Kiminki et al. 2009).

We next consider the fate of the secondary star. If it accreted material from the primary we assume the star is rejuvenated and use its post mass transfer mass as its new initial mass. If a secondary accreted more than 5 per cent of its initial mass when it was a main-sequence star we assume it has been spun up and rotationally induced mixing mixes fresh hydrogen into the core and it is rejuvenated and take it to be a zero-age main-sequence star. We do this at all metallicities. This extends the lifetime of some of our runaway stars. This is a similar assumption as used by Vanbeveren, van Rensbergen & De Loore (1998). If the binary was unbound by the first SN we use a single star model to determine the result of its evolution. If the system

remains bound then we use our secondary models. If the secondary experiences a SN it does so after it has travelled away from the location of the primary SN. We determine the distance travelled by considering in detail the geometry of situation using the runaway velocity relative to the original plane, the orientation of the binary to the line of site, the phase of the stars in the binary and the time that has passed since the first SN. We then record the location of the SN. Finally we determine the final outcome of the binary and whether the system is unbound or a double compact object. We record the velocities of the single and binary compact object.

We perform the above analysis over the full range of our primary models. Because we select our neutron star kicks at random, we repeat our calculations a large number of times to cover the full range of possible outcomes after the first SN.

2.2 Quasi-homogeneous evolution

We include one new evolutionary path, not in the standard picture of binary evolution for our secondary stars. If a secondary accreted more than 5 per cent of its initial mass as discussed above we assume it has been spun up and rotationally induced mixing mixes fresh hydrogen into the core and it is rejuvenated and take it to be a zero-age main-sequence star. If the secondary's initial metal mass fraction is less than or equal to 0.004 and it has a mass after accretion of more than $10M_{\odot}$, we assume it continues to evolve fully mixed during its entire main-sequence lifetime. This is referred to as quasi-homogeneous evolution (QHE). It is the result of rapid rotation due to the accretion of material from the primary star and is described by Maeder (1987), Meynet & Maeder (2007), Yoon & Langer (2005), Yoon, Langer & Norman (2006) and Cantiello et al. (2007). The star does not spin down as at lower metallicity stellar winds are weaker so less angular momentum can be lost.

To include we use simple models in which we assume the stars are fully mixed during their hydrogen burning evolution. Once hydrogen burning ends this extra mixing is turned off. We use the models whether the binary was bound or unbound after the primary SN. We find, at $Z = 0.004$, QHE increases the percentage of SNe that are type Ib/c from 20 to 26 per cent. We find that three per cent of all stars that experience QHE give rise to a long-GRB as we also require a final CO core mass of greater than $7M_{\odot}$ for a long-GRB to occur. More metal rich stars do not experience QHE as we assume the stars rapidly spin-down as the stronger stellar winds take away angular momentum more rapidly.

Our requirement for QHE to occur may seem quite relaxed. Cantiello et al. (2007) restricted their study to a Case B, post-main-sequence mass-transfer system rather than Case A system. This was to avoid orbital synchronization slowing the rotation of the secondary. Therefore we may be overestimating the number of long-GRBs via QHE. However most of the QHE systems in our models are Case B and also systems with high mass ratios which have similar thermal timescales so mass-transfer is most efficient. Therefore the opportunity of tidal synchronization is low. Further more such synchronization is unlikely as the stars have radiative

Table 1. The relative population of mergers from our binary population at different metallicities and with different minimum masses for the binary systems.

Mass Range / M_{\odot}	Z	During MS	Post-MS	No Merger
5 → 120	0.004	0.029	0.001	0.970
	0.020	0.036	0.007	0.957
10 → 120	0.004	0.070	0.002	0.928
	0.020	0.088	0.016	0.896
20 → 120	0.004	0.106	0.005	0.889
	0.020	0.129	0.004	0.867

envelopes during much of their evolution. Thus any tidal forces are likely to be weak.

In addition our 5 per cent increase in mass required for QHE may also seem arbitrary. Only about 10 percent of the mass of a main sequence star needs to be accreted to bring its spin from zero to critical. However QHE does not need critical rotation and the initial rotation rate of these stars is not zero. Therefore 5 per cent is a reasonable limit. A full treatment would require a more detailed model of rotation within the star and the binary. However the inclusion of this would severely limit the stability of the code and thus make it currently difficult to create the large number of models required for population synthesis.

2.3 Non-degenerate mergers

In Table 1 we list the relative fraction of binaries that merge before the first SN occurs. We find that 7 to 10 per cent of binaries with primaries massive enough to explode in a SN experience a merger. Therefore the majority of binaries provide two possible supernova progenitors and contribute to the runaway stars. However even stars not massive enough to provide a SN can merge and in some cases the resulting star is massive enough to produce a SN. We find more mergers in the higher mass binaries.

2.4 Determining SN types

Determining what SN type a star produces is a difficult task. Here we use the relative SN rates of Smartt et al. (2009) to estimate the parameters required for the different types. The rates are based on a volume limited sample of 92 core-collapse SNe within 28 Mpc over 10.5 yrs. The range of metallicities for the SNe tend to be an even mix of LMC and solar like ($Z = 0.008$ and 0.020 respectively). To match the relative rates, we first select out stars that we expect to explode in supernovae. We first require that core carbon burning has occurred and that the total mass of the star is greater than $2M_{\odot}$ and that the carbon-oxygen core mass is greater than $1.38M_{\odot}$. Next we vary the total masses of hydrogen to helium and their relative amounts required for the different SN types. To reproduce the observed rates of Smartt et al. (2009) we find that we must include one single star for every binary system included in the code. Otherwise we cannot reproduce enough type IIP SNe while keeping the maximum type IIP progenitor mass below $20M_{\odot}$. This is the

99 per cent confidence limit on the maximum mass of type IIP progenitors determined by Smartt et al. (2009) from observations. This in effect increases the number of very wide non-interacting binaries in our sample. We summarize the parameters required for each SN type in Table 2. If a type II SN does not produce a IIP event we include it in a broad class of non-IIP SNe. These events are rare and the statistics of Smartt et al. (2009) are not good enough to determine the parameters required for the sub-types of Ib, IIn and III.

For the hydrogen-poor SN-types we differentiate between type Ib and Ic, helium rich and poor SN respectively, by considering the amount of helium in the ejecta. Rather than using the total mass of helium in the ejecta as other authors (Wellstein & Langer 1999; Pols & Dewi 2002; Georgy et al. 2009; Yoon, Woosley & Langer 2010) we consider the fraction of helium in the ejecta to differentiate between Ib and Ic SNe. We prefer this method because otherwise some progenitors with pure helium ejecta of only a fraction of a Solar mass would be identified as Ic rather than Ib. This means our results differ from previous authors. The main difference is that while other authors find two distinct classes of low and high mass type Ic progenitors with type Ib progenitors of mainly low masses, we find more of an overlapping continuum of type Ic and Ib progenitor masses. Drout et al. (2011) suggested this might be the case from a systematic study of lightcurves of type Ib/c SNe. At low metallicity we note more progenitors explode as type Ib SNe. The latter is due to weaker WR winds removing less helium before core-collapse.

The observed relative rates of supernovae from Smartt et al. (2009) are shown along with our synthetic population rates from an equal mix of solar and LMC metallicity in Table 3. The predicted ratios and mean initial masses for the different supernova types are given in Section 3.3. We find that the mean initial mass of the progenitor stars increases through the SN types from IIP being the least massive to Ic progenitors the most massive. The mass ranges of the different SN types are shown in Fig. 1. Type IIP SN progenitors are not only here the lowest mass but also the narrowest range of masses. The remaining SN types have larger ranges of both initial and final mass.

As mentioned above we also record SNe that may have an associated long-Gamma-Ray Burst (GRB) (Woosley & Bloom 2006). While we do not consider rotation in our models, to produce a GRB we require it must have experienced QHE as described above, that the CO core mass must be greater than $7M_{\odot}$ and that the star's rotation axis is within 10 degrees of the line of sight. The direction of the rotation axis is taken to be random. We assume that the rotation axis is perpendicular to the orbital plane. This is important to consider when we calculate the apparent distance travelled by progenitors before they explode as discussed below. Due to our assumptions about QHE, long-GRBs only occur at a metallicity of $Z = 0.004$. One in ten QHE stars leads to a long-GRB and there is one long GRB for every 175 type Ib/c SNe or 685 of all core-collapse SNe. Also we find that the mean initial mass is lower than the mean mass for type Ib and Ic SNe. This is because the stars must accrete mass to be spun up and this biases the progenitors towards lower masses.

Table 2. The required parameters for a star to give rise to a specific SN type.

SN Type	Final Mass / M_{\odot}	CO core Mass / M_{\odot}	$M(\text{H})$ / $M(\text{He})$	$M(\text{H})$ / M_{\odot}	$M(\text{He})$ / $M(\text{ejecta})$
IIP	> 2	> 1.38	≥ 1.1	> 0.05	-
II	> 2	> 1.38	< 1.1	> 0.05	-
Ib	> 2	> 1.38	-	≤ 0.05	≥ 0.58
Ic	> 2	> 1.38	-	≤ 0.05	< 0.58

Table 3. Relative fractions of different SN types from observations of Smartt et al. (2009) and output from our population synthesis with a mix of single stars and binaries at a mix of metallicities.

Z	IIP	non-IIP	Ib	Ic
0.008 & 0.020	0.588	0.122	0.095	0.195
Smartt et al.	0.587	0.120	0.098	0.195

3 RESULTS

While our code can run at any metallicity we restrict ourselves to just two, solar metallicity with a metal mass fraction $Z = 0.02$ and SMC-like metallicity with $Z = 0.004$. This enables us to decouple the effects of metallicity on our results.

3.1 Single-star Runaways

The main output of our code is the distribution of runaway velocities. Observations of runaways have been used to infer that around 10–30 per cent of O stars and 2–10 per cent

Table 4. The fractions of OB stars, red supergiants and Wolf-Rayet stars that are runaways in our synthetic population. We list the fractions from two selection criteria for runaways. First any star that has a peculiar velocity above 5km s^{-1} and a second with a higher velocity requirement of 30km s^{-1} . The former, lower limit, would provide results records runaways in a method similar to the observational method of Stone (1991). We list two populations, one from our standard population including single stars and binaries, and a second including some of the single stars as DES runaways, we assume half the single stars are runaways for half their O star lifetime.

$v_{\text{runaway}} \geq$	$Z = 0.004$		$Z = 0.020$	
	5km s^{-1}	30km s^{-1}	5km s^{-1}	30km s^{-1}
S. & B.				
O	0.161	0.059	0.022	0.005
B	0.069	0.025	0.071	0.022
RSG	0.105	0.020	0.186	0.043
WR	0.496	0.207	0.179	0.029
S., B, & DES				
O	0.190	0.052	0.065	0.015
B	0.093	0.034	0.090	0.028
RSG	0.227	0.046	0.298	0.072
WR	0.506	0.170	0.227	0.020

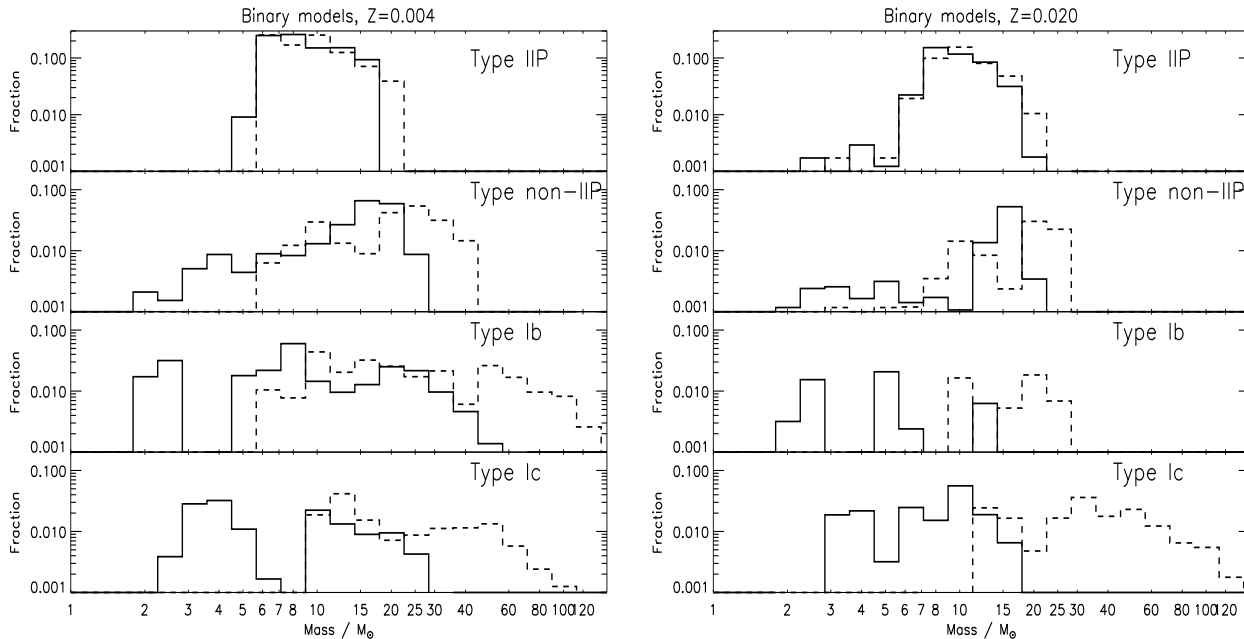


Figure 1. The probability distribution of final (pre-explosion) and initial masses for different type SN progenitors from our population including single stars and binaries. The distribution of initial masses are shown by the dashed lines and the final masses are shown by the solid lines. The models on the left have a metallicity mass fraction of $Z = 0.004$ and the models on the right have a metallicity mass fraction of $Z = 0.020$.

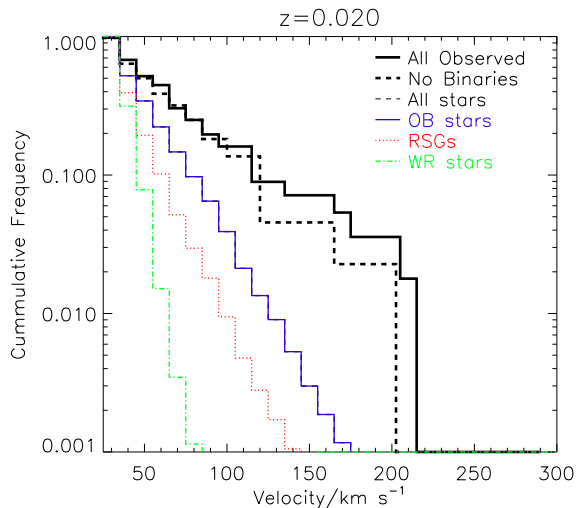


Figure 2. The cumulative frequency of stellar runaway velocities. The thick black line is the observations from Hoogerwerf, de Bruijne & de Zeeuw (2001), the thick dashed line is for the same data but with the known binary stars removed, the thin dashed line is the line predicted by our models for all runaway stars, the blue line for all OB stars, the red line for all red supergiants and the green line for Wolf-Rayet stars. The predictions are for solar metallicity.

of B stars are observed to be runaways (Gies 1987; Stone 1991; de Wit et al. 2005; Zinnecker & Yorke 2007). These observed fractions are very uncertain as the number of well observed runaways is relatively small and the definition of what a runaway is varies between different studies. For ex-

ample the above observed runaway fractions vary because the runaway definition varies between authors. Gies (1987), Stone (1991) and de Wit et al. (2005) state that a runaway must have a velocity greater than 30km s^{-1} or be a large distance above the Galactic plane. Also in some cases it is not clear if the percentage given is the number runaways in the field O star population or the number of runaways relative to the entire O star population.

The recent study of de Wit et al. (2005) suggest the 50 per cent of field O stars are runaways. They also state that since 70 per cent of O stars are in clusters. These facts suggest that possibly 15 per cent of O stars are runaways. They identify runaways by peculiar velocities above 40km s^{-1} , a high distance from the galactic plane or proximity to young clusters. These mixed definitions make it difficult to identify a velocity cut-off to use with our model population to predict the number of runaways. For example even a runaway with a velocity of 5km s^{-1} would travel approximately 10 pc in 1 Myr and would appear as a runaway according to de Wit et al. (2005). Therefore we estimate a range of the fraction of runaways from our models. We use the high velocity of 30km s^{-1} to give a strict minimum runaway fraction estimate and a lower velocity limit of 5km s^{-1} to provide a more relaxed maximum runaway fraction estimate.

In Table 4, we list the fraction of the predicted populations that are runaways. The numbers are calculated weighting each model by its lifetime in the phase of evolution and with a Salpeter IMF. For comparison we list the results for O stars, B stars, red supergiants (RSGs) and WR stars. B stars are taken to be stars with $\log_{10}(T_{\text{eff}}/K) \geq 4.18$ (B5 and earlier only includes stars with initial masses greater than $5M_{\odot}$, the minimum mass of our binary models) and a sur-

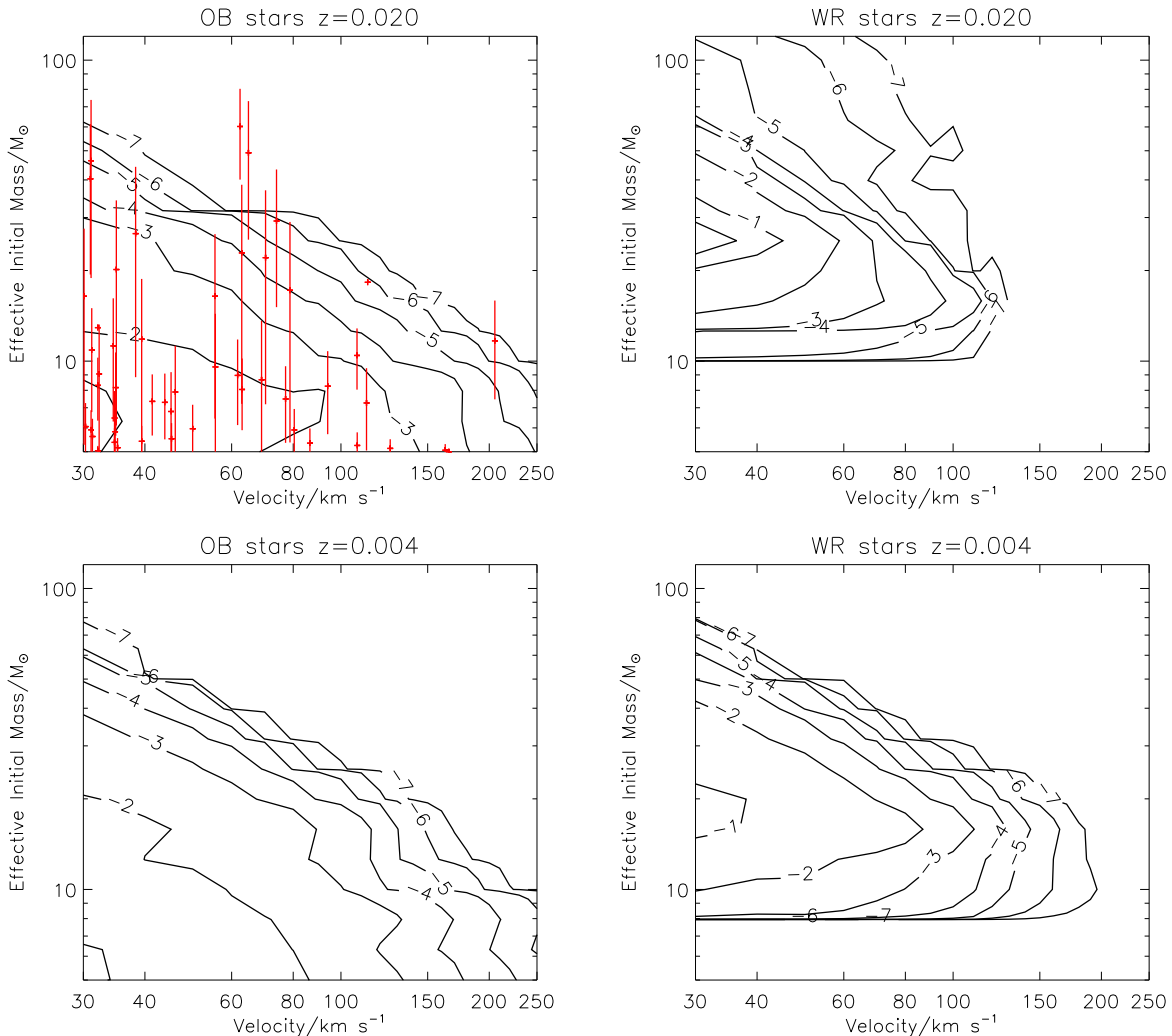


Figure 3. Contour plots of the probability for runaway star to have a certain mass and velocity. The units of the contours are probability per 10 km s^{-1} and per 0.1 in $\log_{10}(M/M_{\odot})$. The mass referred to is the actual mass so includes any mass gained by a runaway during mass transfer. The red points are the observations of OB runaways from Hoogerwerf, de Bruijne & de Zeeuw (2001) with stellar masses derived from fitting the spectral energy distribution. The top two panels are for solar metallicity and the bottom two panels are for SMC-like metallicity. The left hand panels are for OB stars while the right hand panels are for WR stars. The mass axis is either the initial mass of the runaway star or its mass after accretion due to any binary interaction. A similar figure showing the number of stars below the velocity limit for a star to be observed as a runaway, 30 km s^{-1} , is included in the appendix (Fig. 12).

face hydrogen mass fraction greater than 0.4, O stars have hotter effective temperatures of $\log_{10}(T_{\text{eff}}/K) \geq 4.48$ and 4.52 at $Z = 0.020$ and 0.004 respectively. RSGs are defined by $\log_{10}(T_{\text{eff}}/K) \leq 3.66$ and $\log_{10}(L/L_{\odot}) \geq 4.9$ and WR stars are taken to have a surface hydrogen mass fraction less than 0.4, $\log_{10}(T_{\text{eff}}/K) \geq 4$ and the same luminosity limit as the RSGs.

In calculating these numbers we consider count each O, B, RSG or WR star including both the primary or secondary in the binary. It is unclear if in the observed samples an O star binary is counted as one or two O stars. We find 0.5 to 2.2 per cent of O stars are runaways and 2.2 to 7.1 per cent of B stars are runaways at Solar metallicity.

We note that uncertainties in our model may mean the O runaway fraction is an underestimate. For example, the absence of rotational mixing in our stellar evolution models. Rotational mixing mixes fresh hydrogen into the core of

a main-sequence star and this would increase our number of O star runaways by increasing their lifetimes. The evidence that rotation has an importance in the number of O star runaways if we include QHE, the most extreme form of rotational mixing, at solar metallicity the number of O star runaways increases to 2.2 to 16 per cent. We note the dramatic increase in number of O runaways is due to stars, of around $15M_{\odot}$ that have 20 Myrs O star lifetimes with QHE but are not O stars without it. Rotation will have a similar but less dramatic effect at Solar metallicity. The effect of rotation on a stars lifetime is only to increase it by approximately 10 per cent. Including a detailed model of accretion on to the secondary, especially following rotation would allow more accurate inclusion of the effects of rejuvenation on the secondary stars that accrete material from their primaries.

The number of B star runaways is similar to that sug-

gested from observations. We seem to under-predict the number of O star runaways if we compare to the typical numbers quoted for the number of runaway O stars. The work of de Wit et al. (2005) used various O star catalogues including that of Maz-Apellniz et al. (2004). We use the same catalogue to estimate from the catalogue the fraction of O star runaways. It is important to note that we count O star binaries in the catalogue as 2 O stars. We find that 76 ± 5 per cent of O stars are found in clusters with 6 ± 1 per cent of O stars being runaways. The list of runaways includes some binaries, we assume these are DES in origin and find that there are 4 ± 1 per cent of single O star runaways. Considering the uncertainties in classification of runaways and the approximations within our population model our predicted runaway population is comparable to the runaway population in the catalogue of Maz-Apellniz et al. (2004).

Further complicating matters is that we have not considered in our model the contribution of DES runaways. We have made a toy-population assuming that our single star population provide a similar number of DES runaways to the total number of BSS, approximately 30 percent of the binary produce BSS. We then assume that they are runaways for half their O star lifetime and have a similar velocity distribution to the BSS runaways. We see in Table 4 these modest assumptions increase the number of O runaways to between 1.5 to 6.6 and the number of B runaways to between 2.8 and 9 percent. These numbers are also comparable to the observed numbers.

After considering the population of runaways we now consider the velocity distribution and parameters of individual runaways. The best observed sample of OB runaways to date is that from Hoogerwerf, de Bruijne & de Zeeuw (2001) who list the velocities of 56 runaway stars. Hoogerwerf, de Bruijne & de Zeeuw (2001) give masses for some of these estimated by Schmidt-Kaler (1982) and Vanbeveren, De Loore & Van Rensbergen (1998). By using available UVJHK photometry we have employed the methods outlined in Eldridge & Relano (2010) to estimate stellar masses with Cambridge STARS models. Our masses broadly agree with those used by Hoogerwerf, de Bruijne & de Zeeuw (2001) and are used in Fig. 3. The mass range we find is between 5 to $70M_{\odot}$ with half the stars having masses less than $10M_{\odot}$.

In Fig. 2 we plot the cumulative frequency of our runaway population velocities. In general there is agreement between the observed runaway velocity distribution and that predicted by our models. We find that the assumed initial binary separation distribution largely determines the shape of the runaway velocities. Here we use a distribution that is flat in $\log_{10} a$. If we limit ourselves to only close binaries we over predict the number of fast runaways, while considering the widest binaries leads to only the slowest runaways. It appears in the figure that we are under-predicting the number of fast runaways.

Using our estimated initial masses from the runaways we can extend Fig. 2 along another axis as in Figure 3 of *effective* initial mass of the runaway star. This is to take account of the increase in its initial mass due to accretion of mass from its primary companion. The general shape of our predictions is similar to that of Portegies Zwart (2000) who presents a similar figure. In general it is clear that less massive stars are more likely to achieve higher runaway veloci-

ties. The observed runaway stars agree with this prediction however there are several outliers with high masses and moderate velocities. Observations of these stars indicate they also have large rotational velocities, $v \sin i \approx 200 \text{ km s}^{-1}$ (Hoogerwerf, de Bruijne & de Zeeuw 2001), and therefore their masses from SED fitting should be considered upper limits because they were derived with non-rotating single star models. Rotational mixing can increase the luminosity of a star and the main-sequence lifetime. This means their mass would be overestimated and make them more likely to be observed. Alternatively, they could be DES runaways, runaways that experience both DES and BSS or our binary models are producing mergers in very close binaries rather than producing fast BSS runaways from close binaries.

We must be wary of the selection effects of the observed sample. It is easier to observed higher velocity and high mass runaway stars. These selection effects should be more carefully understood before any detailed comparison between observations and theory. For example most runaways are likely to have masses less than $10M_{\odot}$ with velocities below 100 km s^{-1} . However such stars and velocities are difficult to detect within the *Hipparcos* catalogue used by Hoogerwerf, de Bruijne & de Zeeuw (2001). Meanwhile more massive, more luminous stars are easier to detect, especially if they have large proper motions. Quantifying these selection effects is difficult. We may need to wait for the Gaia satellite before obtaining a less biased catalogue of runaway stars. Because the observed population is uncertain we do not attempt further tuning of our initial binary distribution.

We note that at both metallicities the fraction of secondary stars that have accreted some material during mass transfer is 50 per cent. In some cases the amount accreted is very little, only 17 per cent of secondary stars accrete more than 5 per cent their original mass due to assumptions on the maximum accretion rate for the secondary. Because of this we estimate that no more than 50 per cent of BSS runaways should be observed to have high rotation velocities and/or enriched compositions. Therefore, absence of these observable features should not be inferred to mean the runaways did not come from BSS.

Finally we again note that our predictions are for the BSS only. However, the main detail that determines the velocity distribution in both cases is the initial binary separation distribution assumed. We therefore suggest that the expected velocity distribution from the DES should be similar to that of the BSS. Stars that are ejected by DES normally follow the interaction of a binary with another binary or a single star. Gvaramadze & Gualandris (2010) have recently investigated the runaway velocities possible from three body interactions. They found that the mean velocities are similar to those we show here in Figure 2. However they also find the interactions can lead to velocities in excess of 100 km s^{-1} for $80M_{\odot}$ stars in 10 per cent of triple body encounters. This adds weight to the suggestion that runaways more massive than $40M_{\odot}$ with runaway velocities faster than 40 km s^{-1} are in fact DES or a DES+BSS combination.

3.1.1 *Wolf-Rayet runaways*

Fig. 3 shows our results for WR stars. The sharp cut off at low masses in these panels is due to our luminosity limit that WR stars must have $\log_{10}(L/L_{\odot}) \geq 4.9$ to be included.

The difference between the two metallicity plots at higher masses is due to the differing lifetimes of WR stars at the two metallicities. Eldridge & Vink (2006) found that, at SMC-like metallicity, the lifetimes of WR stars vary between 3 to 4×10^5 yrs while at solar metallicity the lifetimes are 4 to 8×10^5 yrs. Furthermore QHE also skews this plot because such stars become WR stars while still on the main sequence and so the plot begins to resemble the OB star panel as the time-scales are millions of years rather than a few hundred thousand years. If we do not include QHE then the distribution becomes the same as for the solar metallicity plot. Thus a large population of runaway WR stars in low-metallicity galaxies with an average velocity above 50 km s^{-1} would be circumstantial evidence for the occurrence of QHE in nature. Surveys for runaways of the SMC have been undertaken but have not yet provided detailed statistics (Gvaramadze, Pflamm-Altenburg & Kroupa 2010).

The fraction of WR and RSG stars that are runaways is larger than the fractions of OB runaways (Table 4). This is because BSS runaway stars spend a large fraction of their main-sequence life stationary, while they spend most or all of the lives as RSGs or WR stars as runaways. This makes their relative number appear greater. At SMC metallicity, the WR runaway fraction is particularly high due to QHE scenario, which produces more WR stars from secondary stars.

The velocities of Wolf-Rayet stars differ strongly between the two metallicities we study. At solar metallicity we find WR runaways have velocities less than about 150 km s^{-1} but runaways with velocities above 80 km s^{-1} are rare. If we do not include black hole kicks we only find WR runaways with initial masses less than $30M_{\odot}$ and 0.4 per cent of WR stars have velocities above 30 km s^{-1} . This is because secondaries that become WR stars owing to stellar wind mass loss have primaries that form black holes at core-collapse and remain bound because very little mass is ejected in such supernovae. We find that WR stars eject relatively little of their final mass, between 2 to $8M_{\odot}$. With such low ejecta masses without a strong kick it is difficult to unbind the binary. It is possible that, due to the sparseness of our binary grid, we may be missing WR runaways from binaries in which both components have initial masses in the range 20 to $25M_{\odot}$. We might also assume too low an initial mass limit for a black hole to be formed in core collapse. Binaries with component masses between 20 and $25M_{\odot}$ may give rise to high velocity runaways as shown by Dray et al. (2005), fig. 2(c), which refers to a similar population synthesis with no black hole kicks. In these systems the binary mass ratio at core collapse is more even so the secondary may achieve a higher velocity. Such systems are still rare and dominated by binary WR stars remaining in their binary systems.

Our results broadly agree with similar theoretical predictions of Dray et al. (2005). It is difficult to perform a quantitative comparison but in their fig. 2(b), which describes their model most similar to ours as it includes black hole kicks, we find broadly similar maximum velocities for WR stars of up to around 120 km s^{-1} . However most WR stars have velocities below 80 km s^{-1} . Dray et al. (2005) also find a restricted number of WR runaways when they assume that black holes do not have kicks.

We note that Dray et al. (2005), in fig. 2(a) predict a large number of runaway WR stars. In this model they ig-

nored stellar-wind mass loss. So more of the secondary stars accrete enough material to become WR stars as single stars, when the stellar wind mass-loss rates are reapplied after the first SN. Such an arrangement is unlikely to occur in nature because, if the metallicity were low enough to reduce the main-sequence mass-loss rates, the minimum mass for a WR star would also increase. The only way for WR stars to occur in such a situation would be via QHE.

Another reason for mostly slow WR runaways in our synthetic population is demonstrated by the example that $50M_{\odot}$ primary stars at solar metallicity form neutron stars in core collapse. These binaries, even with large neutron star kicks, only obtain slow runaway velocities because the secondaries are much more massive than their companions at core-collapse and so their orbital velocities are smaller.

Finally we may also predict more WR runaways if we were to relax our luminosity constraint for a WR star. This number is highly uncertain and if it is set too low we would overpredict the number of WN stars. This would suggest that the higher velocity a runaway WR star has, the lower its initial mass.

Observations of runaway O and WR stars by Moffat et al. (1998) imply that there are a similar fraction of runaways for both types of star. They also suggest that mean kinetic ages based on displacement and motion away from the Galactic plane tend to slightly favour the DES over BSS. There are a few WR stars with higher velocities such as WR 124 with a space velocity of 180 km s^{-1} (van der Sluys & Lamers 2003). Given our results (Fig. 3), it seems unlikely that WR 124 was ejected through the BSS. Conceivably, it may be the result of both DES and BSS combined. Or, as suggested by Moffat et al. (1998), the more massive a runaway the more its probability of coming from DES increases. Recent radio observation by Dzib & Rodriguez (2009) give velocities of about 30 km s^{-1} for a few WR stars, in agreement with our predictions. However they also give a runaway velocity of more than 300 km s^{-1} for WR112, a possible WR+O binary. The high velocity for a binary argues for the highest velocity systems arising from a combination of DES and BSS.

A qualitative method to determine the WR runaway velocity distribution is to consider the orbital velocities of WR binaries with massive O star companions. Using the catalogue of van der Hucht (2001) which lists the masses and periods of many WR binaries we find that, without black hole kicks, many of these binaries are difficult to unbind because the O star is the more massive of the two stars. From the binaries we find typically low velocities, similar to those predicted in Fig. 3, 3 of 10 to 50 km s^{-1} for a $30M_{\odot}$ companion and up to 70 km s^{-1} for a $10M_{\odot}$ companion. Again this leads us to assume that fast and massive WR runaways are most likely to be the result of DES.

3.1.2 Red supergiant runaways

Runaway red supergiants have a similar distribution to the OB runaway stars. It is an interesting question whether such stars could be observed and what would be the structural effects on their envelopes. The most obvious difference may be the distribution of the mass loss in a trail as the star moves in space. A trail has recently been discovered for the red giant Mira which is a low-to intermediate-mass star with a space

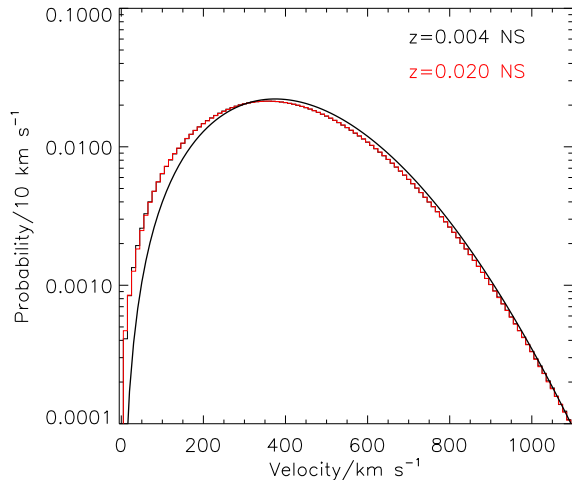


Figure 4. The distribution of runaway velocities for neutron stars. The smooth black line is the input distribution of neutron star kicks. The lines have been normalised so the total probability is 1.

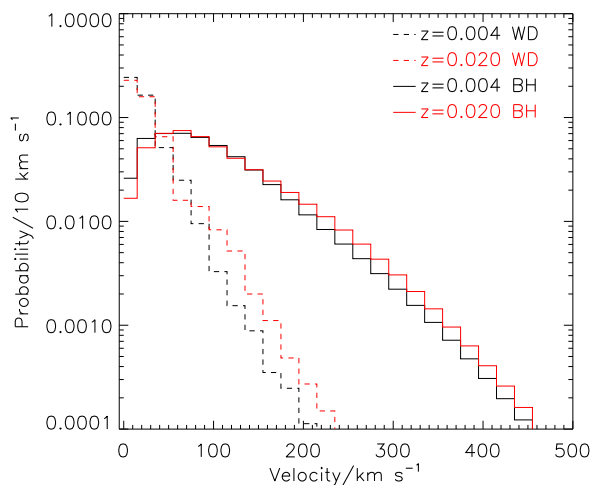


Figure 5. Similar to Fig. 4 but for black holes and white dwarfs.

velocity of 130 km s^{-1} (Martin et al. 2007). Also the closest red supergiant to the Sun, α Ori or Betelgeuse, is a runaway star, which moves with a velocity of about 30 km s^{-1} through its local ISM (Ueta et al. 2008).

3.1.3 White dwarfs, neutron stars and black holes

Finally we consider the velocity distributions for single compact remnants (Fig. 4 and 5). Their relative formation rates and their average space velocities are shown in Tables 6, 7, 8 and 9. We see that it is most likely that stellar remnants are single objects.

The neutron star velocity distribution is dominated by the kick velocity distribution we assume for these objects. At low velocities there is a small excess of neutron stars compared to the input kick velocity distribution. These stars come from binary systems that are not disrupted in the first

SN. Their velocities reflect the orbital velocity of the neutron star in a binary. Thus, when the neutron star kick distribution is estimated from observations, account must be taken of the fact that some of the observed neutron star space velocities are not determined by the neutron star kick. If this is not considered the mean kick velocity may be underestimated and the variance overestimated. Also the upper velocity side of the population is lower than expected. This is because when a binary is unbound as the components separate their mutual gravitational attraction must be overcome. Therefore the neutron stars appear to be travelling slower than they were at birth. We find that we would have to increase the root mean squared velocity used in the Maxwell-Distribution from 265 km s^{-1} to 275 km s^{-1} . We note that here, we do not consider the possibility of a population of low-kick neutron stars emerging from electron-capture supernovae, as advocated by Podsiadlowski et al. (2004).

Neutron stars are our most common runaway compact remnant. Black holes are less populous. We see from Fig. 5 that black holes have a distribution with a peak at around 60 km s^{-1} and most black holes below 250 km s^{-1} . Our rarest runaway remnants are white dwarfs. The distribution is similar to that for all stars in Fig. 2. This is because white dwarfs do not receive any kick and their velocity distribution is representative of their initial binary separations.

We note that with a typical galactic escape velocity of a few times 100 km s^{-1} we can conclude that most white dwarfs and black holes are retained within their host galaxies, while neutron stars are most likely to escape to the intergalactic medium.

3.2 Runaway binaries

The next objects to consider are the runaway binary systems that must contain one or more compact objects. Only 20 per cent of binaries survive the first supernova. Typically these objects have lower velocities than single stars because any kick that did not disrupt the binary must be small and had to transfer momentum to the system rather than just the neutron star.

3.2.1 Stars with a compact companion

If a binary survives the first SN then its velocity relative to the pre-SN centre of mass changes. The neutron star or black hole kick determines this velocity. We see our results in Fig. 6 and there are clear differences between the two types of remnant. The larger neutron star kicks lead to greater velocities so the peak velocity is slightly higher, 60 km s^{-1} rather than 20 km s^{-1} for black hole binaries. The maximum velocities possible by each binary reflect this trend with most black hole binaries having velocities below 200 km s^{-1} while neutron star binaries reaching velocities up to 300 km s^{-1} .

For both compact remnants a reasonable number of these binaries have velocities over 30 km s^{-1} . Therefore a prediction of our code is that such binaries are less likely to be observed within their natal clusters and are more likely to be runaway stars (e.g. Mirabel et al. 2004; Fragos et al. 2009).

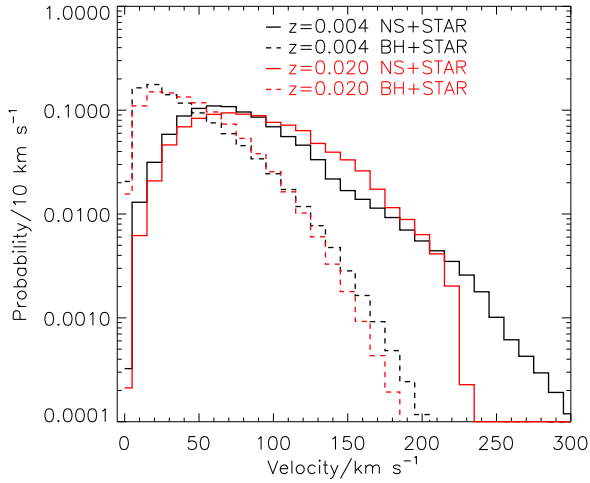


Figure 6. Similar to Fig. 4 but for binaries that contain either a neutron star or black hole. The lifetime of these systems is taken into consideration when calculating the distribution.

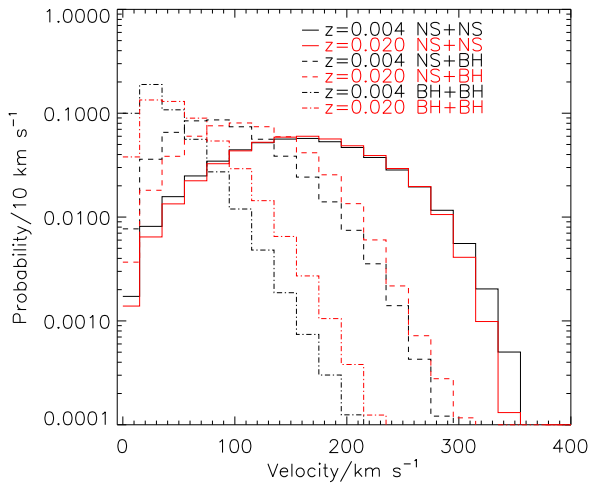
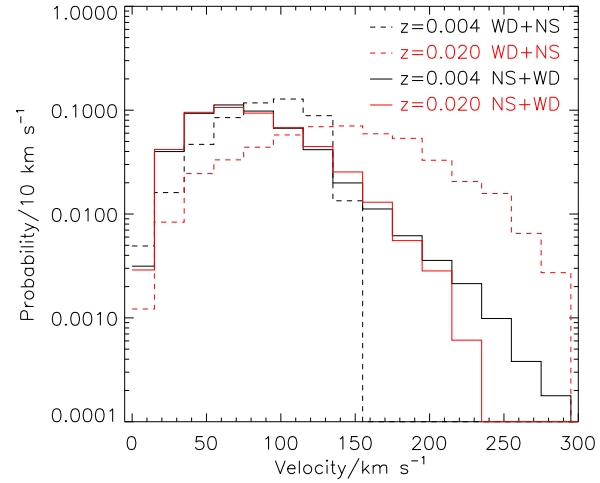


Figure 7. Similar to Fig. 4 but for systems containing two compact objects.

3.2.2 Double compact systems

Systems which experience two SNe are very unlikely to remain bound. There is very little mass left in the system at the time of the second SN, so the system is easily unbound. However the more massive the remnant from the first SN the more likely the binary is to remain bound but the slower the resultant binary will move. The relative birth rates of different single and binary compact remnants are listed in Tables 6 and 8 and this trend is clear with there being more black-hole primary compact binaries than neutron-star primary binaries. Furthermore in Tables 7 and 9 the mean velocities of neutron-star primary systems is greater than that when the primary produces a black-hole.

Further insight into the nature of compact binaries can be seen in Fig. 7. There is a trend through the distributions from only low space velocities for double black-hole binaries

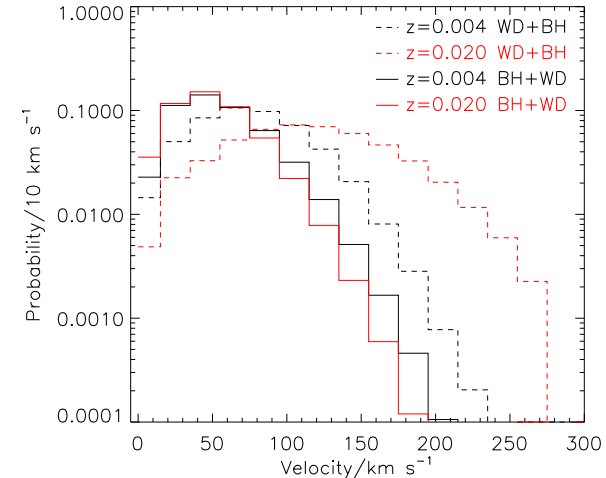


Figure 8. Similar to Fig. 4 but for systems containing a compact object and a white dwarf.

to the highest velocities for double neutron-star binaries. This demonstrates the most important fact for the remnant velocities is the number of large neutron-star kicks a binary receives.

As mentioned in Section 3.1.3, these velocity distributions imply that double neutron-star compact binaries may be able to escape their host galaxy because of they experience at least one large kick compared to double black hole binaries which should be retained by most galaxies.

3.2.3 White dwarf systems

For completeness we have also included the systems that contain a white dwarf and a neutron star or black hole. We find in most of these systems the white dwarf forms second. The velocity distribution is determined primarily by the kick given to the neutron star or black hole at its formation.

Systems that form white dwarfs first and then neutron stars or black holes due to mass transfer are rare. This is to be expected because white dwarfs have low mass and, unless the kick is small or occurs in a small restricted set of direc-

tions, the system becomes unbound. The runaway velocity of such systems is greater than systems that experience the SN before the WD is formed. This is because while the systems are easier to unbind because of their low system mass they are also easier to accelerate to high velocities. Therefore the peak velocity of these systems is higher and provides an observational signature of such systems. The fact that we model some such systems indicates that we are producing SNe from secondary stars that accrete material to end their life in SNe rather than as white dwarfs.

3.3 Supernovae and gamma-ray bursts

With the velocities of the runaway stars and their lifetimes as runaways we calculate the distance that stars may travel before their explosive deaths. This may help to qualitatively interpret recent observations concerning the environments and locations within the host-galaxy of core-collapse SNe and gamma-ray bursts. For example Fruchter et al. (2006); James & Anderson (2006); Kelly, Kirshner & Pahre (2008) and Anderson & James (2008) resolve the host galaxy at resolutions of hundreds of parsec. Determining how different supernovae types are distributed relative to the light of a galaxy. Hammer et al. (2006) studies the host galaxies with greater resolution, calculating the distance between long-GRBs and the nearest region containing WR stars. We calculate the distance a progenitor travels by multiplying the runaway velocity of the progenitor by the time spent as a runaway. To calculate the apparent distance observed on the sky we also take account of the random orientation of the plane of the binary and the phase of the two stars in the orbit. When we calculate the apparent distance we also take into consideration the three dimensional motion of the runaway relative to the original binary orbit as given by the formulae of Tauris & Takens (1998).

We analyze our results in two different forms. First we arrange the SN progenitors by the type of SN we predict the star produces and secondly we consider how distance varies with initial mass. Our results are shown in Tables 10 and 11 showing the predicted ratios, mean *effective* initial mass, runaway velocity, distance travelled and ages before core-collapse for the different SN types and progenitor sources. In calculating the distance travelled we neglect the galaxy potential. Therefore the furthest distances that we predict may be modified if this was considered (Voss & Tauris 2003). We note the distance distributions are non-Gaussian and thus the mean distances give here should be considered with care. In these tables there are also some surprises. For example in Table 11 the mean mass of type Ic SNe decreases relative to the higher metallicity mass in Table 10. This is primarily due to the inclusion of QHE changing the outcome of lower mass stars and also that the highest mass stars retain enough helium to become type Ib rather than type Ic (see Figure 1).

Using the method outlined in Section 2.4 above we are able to create Fig. 9 and 10 showing the distances travelled by progenitors of different SN types from our binary models alone. There are also panels showing how the different progenitor masses contribute to the combined distributions. We only consider binaries because we have not included DES runaways in our model. If the number of runaways is similar from DES as for BSS then the distribution of SNe for the

latter should be similar to that for the combined runaway population.

On first inspection of Figures 9 and 10 we see that most SNe occur at their initial location. This is no surprise because 60 per cent of SNe from binaries are from the primary star, with only 40 per cent coming from secondary stars which are the most likely to travel any distance from their initial location. Primary stars dominate the statistics because this also includes merged systems. These increase the number of primary stars that have an effective initial mass great enough to produce a SN and decrease the number of secondary stars available to produce a supernova. The latter effect further boosts the apparent contribution of single stars to the total number of SNe.

The property that most affects the range of runaway distances for a specific SN type is the mass range of the progenitors. Type IIP come from stars with masses below $20M_{\odot}$, which travel great distances due to their long lifetime. The other SN types typically have higher maximum initial masses and wider mass ranges (see Fig. 1) which lead to the different distributions to those in the Figs. In the solar metallicity plot in Fig. 9 we see that type Ib SNe have a similar distribution to type IIP SNe because most progenitors come from the same initial mass range. This similarity is weaker at the lower metallicity because it becomes swamped by the stars with QHE. This is also evident from the mean initial mass of the different progenitors in Tables 10 and 11.

Type Ic SNe typically occur closer to their initial positions than type IIP and Ib SNe. It is difficult to find observations with which these predictions can be tested. Use of the observations of discussed above would require some knowledge of the luminosity of the source stellar population, star formation history and the galactic potentials through which the runaway stars travel. Also, as yet, these studies do not consider the selection effects of detecting supernovae in luminous and dusty regions of galaxies. For example, type Ib/c supernovae are generally more luminous than type IIP supernovae, although there is significant diversity in the SN population (Richardson et al. 2002). If this difference was true then type Ib/c would be more easily discovered in luminous regions of galaxies where type IIPs might be missed. Thus some of the observed difference in the distributions of different supernova types could be due to the intrinsic luminosities of these objects and selection effects.

When we consider that the resolution which Kelly, Kirshner & Pahre (2008) resolves typical galaxies in their samples is only a few hundred parsecs. Therefore it is the relative distributions beyond these distances are important. Our results in Figures 9 and 10 do therefore qualitatively agree with the findings of Kelly, Kirshner & Pahre (2008) that, in general terms, type IIP and Ib SNe should be less correlated with star-formation in a galaxy than type Ic SNe, especially in environments with solar metallicities. This is because type II and Ib SNe travel similar distances because the age and mass ranges at which these SNe occur overlap. In comparison the ages for type Ic SNe are considerably lower. The type Ic SNe do not travel so far from their birthplaces because they arise from the most massive progenitors. This is in addition to the lifetimes of the progenitors of typical IIP and Ib SNe being similar and longer than those of type Ic SNe.

3.4 Long gamma-ray bursts

In conjunction with studying SNe we consider the predicted distribution for long-duration GRBs and we relate this to quasi-chemically homogeneous evolution (Sect. 2.2). While Yoon, Langer & Norman (2006) relate long-duration GRBs to the quasi-chemically homogeneous evolution of rapidly-rotating single stars, we consider only the binary-induced quasi-chemically homogeneous evolution as explored by Cantiello et al. (2007). This has the advantage that the predictions do not depend on the initial distribution function of stellar rotation rates. This also means that we predict a wider range of initial masses for long-GRB progenitors than Yoon, Langer & Norman (2006). For their single star models stars would lose significant angular momentum before core-collapse, even at lower metallicities than we study here. In our model because the stars are spun up they can retain more angular momentum until core-collapse. Because of this we may be overestimating the number of very massive (greater than $60M_{\odot}$) long-GRB progenitors. If we have fewer of these objects it would increase the mean distance travelled by the progenitor stars given in Table 11.

We find that long-duration GRBs have a bimodal distribution of distances. First, 20 per cent explode without travelling any distance. These are from binaries where the primary star does not explode or the supernova order has been reversed. Then a second distribution travels on average a few hundred parsecs before exploding. This second group of long-GRBs are constrained to greater apparent distances because of the requirement that the binary orbit must be perpendicular to the line of sight for the GRB to be observed. Their distribution is also similar to that for type Ic, as suggested by Fruchter et al. (2006) and Kelly, Kirshner & Pahre (2008). While at the same time as shown in Figure 10 the maximum distances possible are smaller than those of other SNe. In addition many of our possible GRB progenitors travel a few hundred parsecs from their initial location. This is in agreement with the observations of Hammer et al. (2006) who find such distances for some near by GRB progenitors. Initially this result may appear at odds with the observations of Fruchter et al. (2006) but as mentioned the maximum distance that can be travelled would be unresolved in their observations so GRBs would be expected to occur associated with regions of the most intense star formation.

Also we note from Fig. 10 that lower mass long-GRB progenitors are more likely to travel further than high mass progenitors. The nearby long-GRBs considered by Hammer et al. (2006) are relatively weak compared to normal cosmological GRBs (Woosley & Bloom 2006). It is possible that the nearby bursts come from lower mass progenitors than the high redshift long-GRBs. However such a deduction is uncertain and cannot be investigated with our simple model.

We have also varied our requirement that the final CO core mass must be greater than $7M_{\odot}$ for a long-GRB to occur. For example if we restrict long-GRB to have CO core masses at core-collapse of $5M_{\odot}$ rather than $7M_{\odot}$ as in our fiducial model then the mean distance travelled by long-GRBs increased to 240 ± 380 pc. The mean effective initial mass and lifetimes also change to $21 \pm 14M_{\odot}$ 43 ± 25 Myrs. These differences are because the long-GRB

population is more dominated by the lower mass QHE progenitors. We find qualitatively that if such a population represented the observed population then long-GRBs would be the most widely distributed explosive transient of all core-collapse events. Therefore our predicted long-GRB progenitor population is strongly dependent on the approximations included in our simulation.

Two studies which used the results of Fruchter et al. (2006) to determine a limit on the progenitors of long-GRBs were by Larsson et al. (2007) and Raskin et al. (2008). They found that they could explain the results of Fruchter et al. (2006) if the initial mass of GRB progenitors is greater than $20M_{\odot}$ and $43M_{\odot}$ respectively (with lifetimes of 10Myrs and 5Myrs). They did not consider the effect of runaway stars in this analysis. Our results on GRB progenitors in Table 11 show that GRB progenitors may have effective initial masses of $41 \pm 17M_{\odot}$ (or an initial mass of $27 \pm 16M_{\odot}$ before mass accretion). Because the stars can accrete mass from their primary companion the lifetime of these possible progenitors is 15 ± 5 Myrs, three times the age normally expected for stars of this mass. This is greater than the maximum age predicted by Larsson et al. (2007) and Raskin et al. (2008) for the progenitors of long-GRBs. The greater age is due to the QHE increasing the main-sequence lifetime and rejuvenation of the stars. Our result therefore agrees with the mass of Raskin et al. (2008) but disagrees with their age as it is too low. While the mass of Larsson et al. (2007) agrees with the initial mass of our progenitors before mass accretion is considered and is closer to our age estimate.

Qualitatively, because of the uncertainties of what is required to cause a long-GRB and the effect of DES runaways on our results, our model is consistent with the observations of the locations of SNe and long-GRBs. Quantitative analysis however require involving our runaway models with a more detailed galactic model that also considers the stellar populations (that consider binaries) that give rise to these events.

3.5 Merger events of compact-object binaries

We have also calculated similar plots as in the previous subsection for mergers of the compact remnant binaries we discuss in Section 3.2.2. We use the general relativistic weak-field approximation equation employed by Hurley, Tout & Pols (2002) to calculate the time for such binaries to merge via gravitational radiation. We then only count it as a merger if the time we estimate is less than 13.5 Gyrs.

Our calculations are based on the present day population. I.e., they do not include a realistic simulation of the changing populations over cosmological times. Our results should thus hold as long as most systems merge within the age of the Universe. As shown below, this is mostly the case.

We show the distribution of merger times in Fig. 11. We see that it is more probable that a system takes a long time to merge. However there are also systems that have extremely short merger times and so could merge within star formation regions. These results mirror those of Dewi & Pols (2003), Voss & Tauris (2003), Belczynski et al. (2006) and O'Shaughnessy et al. (2008).

Over a similar range of merger times Belczynski et al. (2006) have two sharply defined peaks in the merger rate at

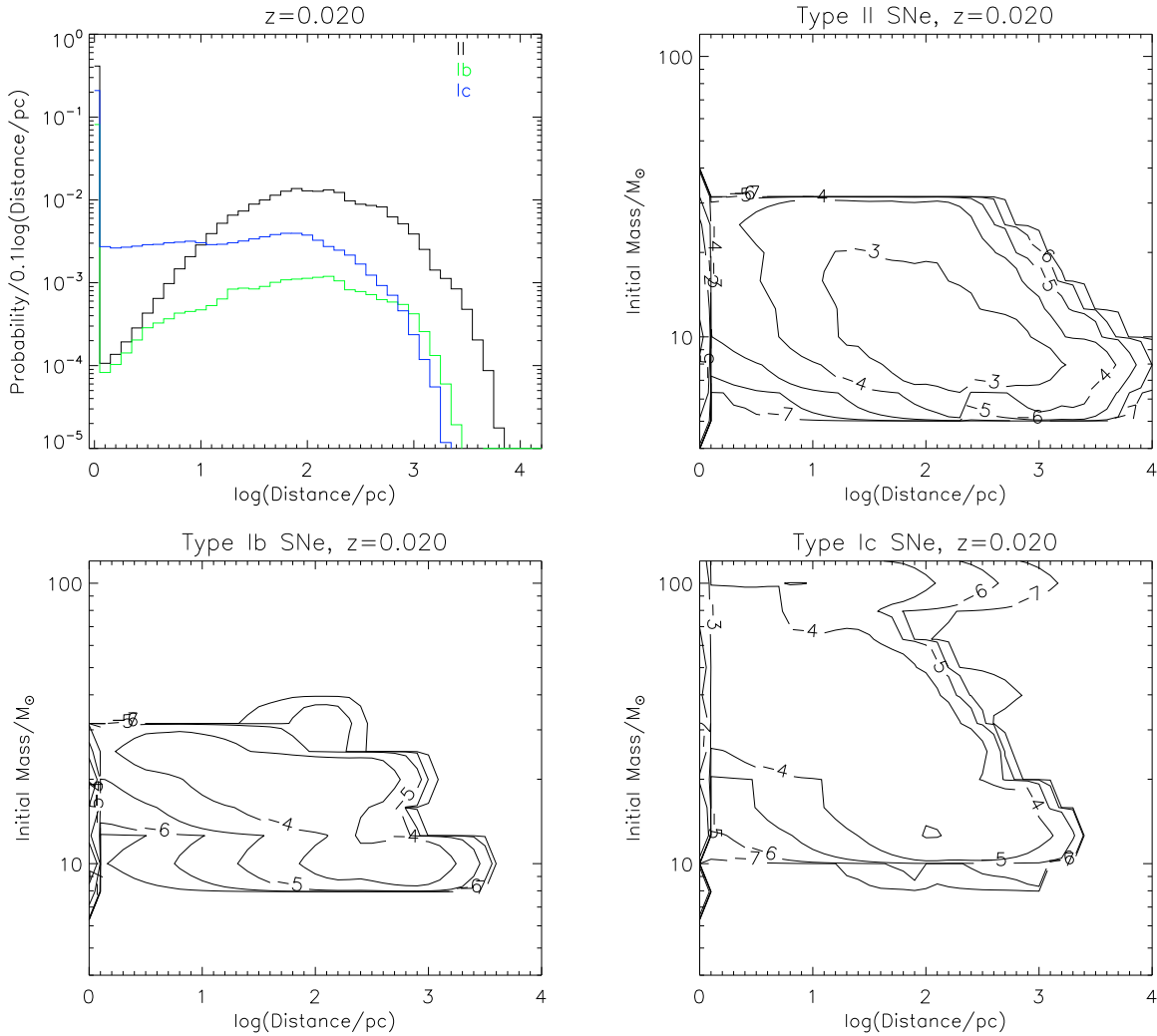


Figure 9. The distribution of distances travelled by different SN progenitors arranged by SN type and initial mass from our binary models alone. The lines and contours are normalised so the total number of SNe is 1. The plots are for solar metallicity. Contours are $\log_{10}(\text{probability}/M_{\odot} \text{ pc})$

around 10^5 and 10^9 years. They found that the two peaks correspond to two different compact binary formation scenarios. In the first each star experiences one mass transfer episode while in the second the secondary experiences an extra mass transfer episode when it becomes a helium giant. This second scenario leads to the tightest binaries and thus the shortest merger times. We do not find such a sharply defined peaks however our range of possible times is comparable. We may be incorrectly estimating some of the merger times due to our basic treatment of the gravitational radiation and assumption of circular orbits in the stellar models.

The merger rates, shown in Table 5 and Fig. 11, indicates that merging black holes and neutron stars are the most common visible mergers. However we are not able to estimate the merger rates for systems containing white dwarfs due to limitations of our grid of models for the secondaries evolution. We are able to calculate the birthrate and give this in Table 5. If a similar number of these systems merge within the age of the universe as for the other compact binaries then the rate of white dwarf-neutron star or black

Table 5. Predicted rates of binary compact object mergers and births relative to the rate of core collapse supernovae, at the two considered metallicities.

Z	WD-NS	WD-BH	NS-NS	NS-BH	BH-BH
Compact-system merger rate					
0.004	–	–	0.00007	0.0017	0.0019
0.020	–	–	0.00009	0.0008	0.0021
Compact-system birth rate					
0.004	0.0045	0.0078	0.0003	0.0052	0.0292
0.020	0.0054	0.0074	0.0004	0.0029	0.0181

hole mergers may be greatest. The rate of such mergers must be less than 1/80th of the core collapse supernova rate. Thompson et al. (2009) suggest a rate between 1/20th and 1/40th of the SN rate from the observation of one such system. Because the observable outcome of such events is not yet well studied (Paschalidis et al. 2009), it seems unclear whether they have observable counterparts. We suggest that

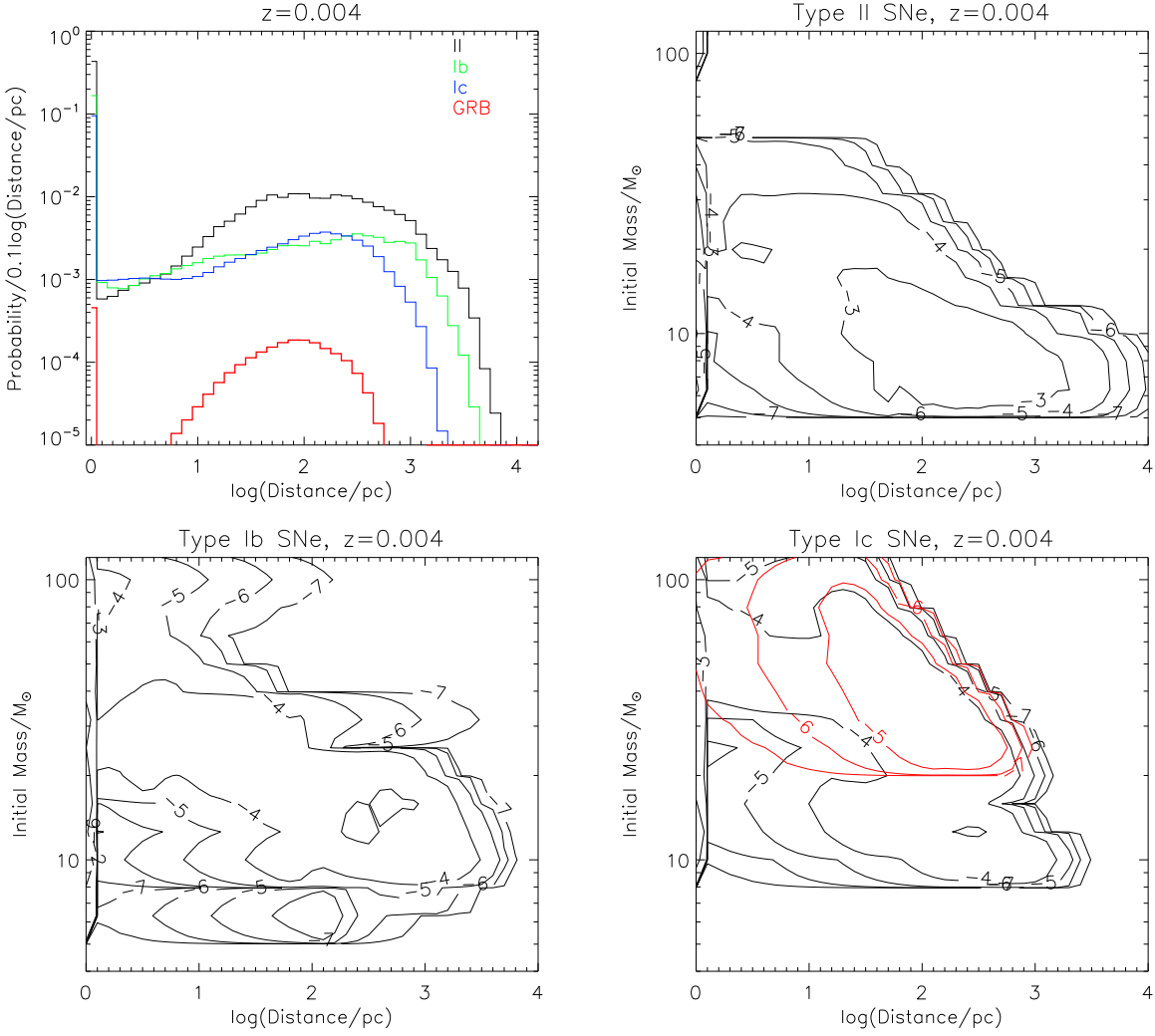


Figure 10. Similar to Figure 9 but now SMC-like metallicity. The red contours in the lower right panel indicate that distribution for long-GRB progenitors.

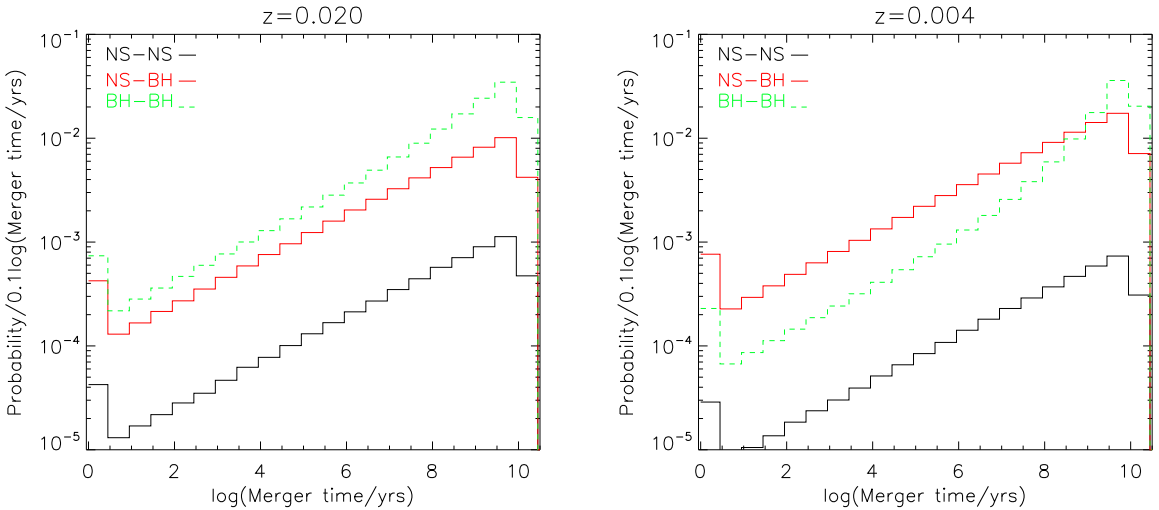


Figure 11. The distribution of time required for compact binaries to merge. The lines are normalised so the total number of mergers is one.

it is possible for these systems the merger is most likely to be an extended period of mass transfer. When the white dwarf is less massive than the neutron star any mass transfer is sufficiently stable (Tout et al. 1997) so these binaries might be observed as X-ray binaries with mass-transfer driven by gravitational radiation.

When we consider where compact binary merger events might be observed we should bear in mind the results displayed in Fig. 7. Here we find that many compact binaries have high space velocities and can escape their host galaxies, especially double neutron-star systems. Therefore we should expect some compact-object binary merger events to occur some distance away from any nearby galaxy. There is growing evidence that some such events do occur (Levan 2007; Salvaterra et al. 2010). Merging double-neutron star systems as well as neutron star-black hole mergers are possibly related to short gamma-ray bursts. In this case these rates should be considered upper limits on the observable rate because the progenitor rotation axis must be within a small angle to the line of sight to be observed, just as for the long-GRBs.

4 DISCUSSION & CONCLUSIONS

Our population synthesis of runaway stars is able to predict a velocity distribution similar to that observed for OB stars. We predict that in the Galaxy the number of all O stars that are runaways from BSS is between 0.5 to 2.2 per cent. Using the catalogue of Maz-Apellniz et al. (2004) we estimate the observed number is 4 ± 1 per cent, however both numbers are uncertain and very sensitive to the total number of O stars in the sample and how runaways are identified.

While we do not consider dynamical ejection from clusters here, we suggest that this distribution may be similar to that predicted for the binary supernova ejection scenario. This is because stars ejected by dynamical interactions in a cluster are normally the result of binary interactions so that the determining factor for both scenarios is the initial separation distribution of binary stars. The initial binary period/separation distribution has a direct effect on the velocities of runaway stars. A wide range of binary separations is required to explain the observed velocity distribution. A distribution that is flat in the logarithm of the separation reproduces the observed range of runaway velocities. However this separation distribution may underestimate the number of close binaries.

To match the fact that there are a number of observed WR runaways with velocities greater than 30 km s^{-1} we include black hole kicks when black holes are formed by core-collapse. This has implications for the velocities of binaries that include a black hole. These should be more often observed as runaways. For example the X-ray binary Nova Sco which has a space velocity of $150 \pm 19 \text{ km s}^{-1}$ provides evidence that at least some black holes may have kicks at their formation. Nelemans et al. (1999) suggest that such large velocities for black-hole binaries do not require a large kick. From the black-hole binaries they list we find the mean velocity is $34 \pm 32 \text{ km s}^{-1}$, this is similar to the distribution of synthetic black hole binaries shown in Figure 6.

We consider the final outcome of our stars and the velocity distribution of compact stellar remnants. Our models

predict that there should be a small surplus of neutron stars with space velocities less than 200 km s^{-1} . These require a system not to be unbound by the first SN but by the second. If these were not taken into account when the neutron star kick is determined from observations it would lead to an underestimate of the kick velocity. Most white dwarfs and black hole runaways have velocities typically below those expected for neutron stars. The final outcome of evolution of all our binaries is that most compact stellar remnants are single. Only 20 per cent of all binaries that experience at least one SN remain bound. The rarest are white dwarf and neutron star binaries where the white dwarf formed first. Normally such systems can be identified by their highly eccentric orbits, for example PSR B2303+46 and PSR J1141-6545 (Kaspi et al. 2000; van Kerkwijk & Kulkarni 1999). There is a predicted difference in the space velocity between such binaries and those in which the neutron star forms first.

Whether a SN progenitor is a runaway star is an important factor in where a SN might occur in a galaxy. We have shown that less massive stars travel further from their initial positions than more massive stars. However the majority of stars explode without travelling a large distance. When we consider the different SN types we find that because type II and type Ib SNe come from progenitors less massive than $20M_{\odot}$ they can travel furthest from their initial positions, $48 \pm 210 \text{ pc}$ and $34 \pm 150 \text{ pc}$ respectively on average. While type Ic progenitors come from more massive stars and therefore have shorter lifetimes and travel shorter distances, $17 \pm 74 \text{ pc}$. This picture changes at low metallicity with the inclusion of quasi-homogeneous evolution, which prolongs the life and the distance to which type Ic and type Ib progenitors can travel.

Nearly one third of long-GRB progenitors may travel a few hundred pc from their birthplaces before experiencing core-collapse. But, they can travel shorter distances and/or explode before type IIP and Ib SNe and so should be the most tightly correlated with star-formation in the host galaxies. These distances however are dependent on the parameters taken for a model to give rise to a long-GRB.

Type IIP supernova progenitors that are secondaries in a binary are distributed throughout a galaxy due to BSS more than progenitors of long-GRBs. These remain closer to their birth places and have shorter lifetimes so explode when the star-formation episode they belong to is still visible Larsson et al. (2007); Raskin et al. (2008). Therefore these effects in combination can explain the observed distribution of SN within galaxies. To infer the nature of long-GRB progenitors from such observations runaway stars must be considered. We find that of the supernovae in Tables 10 and 11, 20 per cent of the SN come from BSS runaway stars. If there are at least as many DES runaway progenitors then between 20 to 40 per cent of SNe has a progenitor that was runaway star. A similar fraction was suggested from observations by James & Anderson (2006). Without considering the effect of runaway stars, the mass of long-GRB progenitors is likely to be overestimated.

Neutron star-black hole binaries and more so double neutron star systems, which are candidate short-GRB progenitors, are found to reach large runaway velocities. We estimate their merger timescales and find that they should often merge outside of their host galaxy. Compact mergers of a white dwarf with either a neutron star or black hole

are estimated to be at least as common as other compact binary mergers. Due to their low runaway velocities and merger timescales, they should mostly merge within their host galaxy. The observational signature of such events appears to be as yet unclear.

5 ACKNOWLEDGEMENTS

We would like to thank the constructive input from the anonymous referee. JJE is supported by the Institute of Astronomy's STFC Theory Rolling Grant. CAT thanks Churchill College for his Fellowship. Thanks to V. Gvaramadze and Thomas Tauris for discussions.

REFERENCES

- Anderson J.P., James P.A., 2008, MNRAS, 390, 1527A
 Belczynski K., Perna R., Bulik T., Kalogera V., Ivanova N., Lamb D.Q., 2006, ApJ, 648, 1110
 Blaauw A., 1961, BAN, 15, 265B
 Brandt N., Podsiadlowski P., 1995, MNRAS, 274, 461B
 Brandt W.N., Podsiadlowski Ph., Sigurdsson S., 1995, MNRAS, 277L, 35B
 Cameron A.G.W., Mock M., 1967, Natur, 215, 464C
 Cantiello M., Yoon S.-C., Langer N., Livio M., 2007, A&A, 465L, 29C
 Crockett R.M., 2008, MNRAS, 391L, 5C
 Dewi J.D.M., Pols O.R., 2003, MNRAS, 344, 629D
 de Donder E., Vanbeveren D., van Bever J., 1997, A&A, 318, 812
 de Donder E., Vanbeveren D., 2003, NewA, 8, 817D
 de Donder E., Vanbeveren D., 2004, NewAR, 48, 861
 de Jager C., Nieuwenhuijzen H., van der Hucht K. A., 1988, A&AS, 72, 259D
 de Wit W.J., Testi L., Palla F., Zinnecker H., 2005, A&A, 437, 247D
 Dray L. M., Dale J. E., Beer M. E., Napiwotzki R., King A. R., 2005, MNRAS, 364, 59D
 Drout M.R. et al., 2011, ApJ in press
 Dzib S., Rodriguez L.F., 2009, arXiv 0902.2962D
 Eggleton P.P., 1971, MNRAS, 151, 351
 Eldridge J.J., Relano M., 2010, Submitted to MNRAS
 Eldridge J.J., Tout C.A., 2004a, MNRAS, 348, 201
 Eldridge J.J., Tout C.A., 2004b, MNRAS, 353, 87
 Eldridge J.J., Vink J.S., 2006, A&A, 452, 295
 Eldridge J.J., Izzard R.G., Tout C.A., 2008, MNRAS, 384, 1109E
 Eldridge J.J., Mattila S., Smartt S.J., 2007, MNRAS, 376L, 52E
 Evans C. J. et al., 2010, ApJ, 715L, 74
 Fragos T., Willems B., Kalogera V., Ivanova N., Rockefeller G., Fryer C.L., Young P.A., 2009, ApJ, 697, 1057
 Freire P.C.C., 2010, MNRAS in press
 Fruchter A.S., 2006, Natur, 441, 463F
 Garmany C. D., Conti P. S., Massey, P., 1980, ApJ, 242, 1063G
 Georgy C., Meynet G., Walder R., Folini D., Maeder A., 2009, A&A, 502, 611G
 Gies D.R., 1987, ApJS, 64, 545G
 Gvaramadze V.V., Gualandris A., 2010, MNRAS, tmp, 1475
 Gvaramadze V.V., Pflamm-Altenburg J., Kroupa P., 2010, arXiv, 1010.2490
 Hammer F., Flores H., Schaerer D., Dessauges-Zavadsky M., Le Floch E., Puech M., 2006, A&A, 454, 103H
 Hansen B.M.S., Phinney E.S., 1997, MNRAS, 291, 569H
 Heber U., Edelmann H., Napiwotzki R., Altmann M., Scholz R.-D., 2008, A&A, 483L, 21H
 Heger A., Fryer C.L., Woosley S.E., Langer N., Hartmann D.H., 2003, ApJ, 591, 288
 Hirschi R., Meynet G., Maeder A., 2004, A&A, 425, 649
 Hobbs G., Lorimer D.R., Lyne A.G., Kramer M., 2005, MNRAS, 360, 974H
 Hoogerwerf R., de Bruijne J.H.J., de Zeeuw P.T., 2001, A&A, 365, 49H
 Hurley J.R., Pols C.A., Tout O.R., 2000, MNRAS, 315, 543H
 Hurley J.R., Tout C.A., Pols O.R. 2002, MNRAS, 329, 897
 James P.A., Anderson J.P., 2006, A&A, 453, 57
 Kalogera V., 1999, ApJ, 521, 723K
 Kaspi V.M. et al., 2000, ApJ, 543, 321
 Kelly P.L., Kirshner R.P., Pahre M., 2008, ApJ, 687, 1201K
 Kiminki D.C., Kobulnicky H.A., Gilbert I., Bird S., Chunev G., 2009, AJ, 137, 4608K
 Kobulnicky H., Fryer C.L., 2007, ApJ, 670, 747K
 Kudritzki R.P., Pauldrach A., Puls J., 1987, A&A, 173, 293
 Larsson J., Levan A.J., Davies M.B., Fruchter A.S., 2007, MNRAS, 376, 1285
 Levan A.J., 2007, RSPTA, 365, 1315L
 Maeder A., 1987, A&A, 178, 159M
 Maz-Appelnicz J., Walborn N.R., Galu H. , Wei L.H., 2004, ApJS, 151, 103M
 Martin D.C., 2007, Natur, 448, 780M
 Meynet G., Maeder A., 2007, A&A, 464L, 11M
 Mirabel I.F., Mignani R., Rodrigues I., Combi J.A., Rodriguez L.F., Guglielmetti F., 2002, A&A, 395, 595M
 Mirabel I.F., Rodrigues I., Liu Q.Z., 2004, A&A, 422L, 29
 Moffat A.F.J., et al., 1998, A&A, 331, 949M
 Nelemans G., Tauris T.M., van den Heuvel E.P.J., 1999, A&A, 352L, 87N
 Nugis T., Lamers H.J.G.L.M., 2000, A&A, 360, 227
 Petrovic J., Langer N., van der Hucht K.A., 2005, A&A, 435, 1013P
 O'Shaughnessy R., Kim C., Kalogera V., Belczynski K., 2008, ApJ, 672, 4790
 Paschalidis V., MacLeod M., Baumgarte T.W., Shapiro S.L., 2009, PhRvD, 80, 4006
 Pflamm-Altenburg J., Kroupa P., 2010, MNRAS, tmp, 348P
 Pinsonneault M.H., Stanek K.Z., 2006, ApJ, 639L, 67P
 Podsiadlowski P., Langer N., Poelarends A.J.T., Rappaport S., Heger A., Pfahl E., 2004, ApJ, 612, 1044
 Pols O.R., Tout C.A., Eggleton P.P., Han Z., 1995, MNRAS, 274, 964
 Pols O.R., Dewi J.D., 2002, PASA, 19, 233P
 Portegies Zwart S.F., 2000, ApJ, 544, 437
 Raskin C., Scannapieco E., Rhoads J., Della Valle M., 2008, ApJ, 689, 358R
 Richardson D., Branch D., Casebeer D., Millard J., Thomas R.C., Baron E., 2002, AJ, 123, 745R

Table 6. The relative birth rates of binary-produced unbound compact objects (white dwarfs, neutron stars and black holes), and compact objects which remain part of a binary system, compared to the birth rate of single compact objects (last line). For compact objects remaining in binaries, it is distinguished whether they form from the primary or the secondary star. These results refer to our population synthesis model at a metallicity of $Z=0.020$. The columns indicate the remnant from the primary star of the binary with the rows referring to the remnant from the secondary star.

	Unbound	Primary WD	Primary NS	Primary BH
Unbound		0.0176	0.1397	0.0747
Secondary WD	0.0280	0.1634	0.0032	0.0045
Secondary NS	0.0916	0.0002	0.0003	0.0013
Secondary BH	0.0354	0.0001	0.0005	0.0112
Single		0.1831	0.1481	0.0972

Table 7. The mean space velocities of different single and binary compact remnants at a metallicity of $Z=0.020$.

	Unbound	Primary WD	Primary NS	Primary BH
Unbound		11 ± 3	420 ± 180	100 ± 70
Secondary WD	24 ± 18	0	81 ± 38	51 ± 27
Secondary NS	390 ± 180	140 ± 55	160 ± 62	110 ± 45
Secondary BH	100 ± 67	120 ± 53	110 ± 52	53 ± 32
Single		0	430 ± 190	96 ± 61

Table 8. The relative birth rates of different single and binary compact remnants at a metallicity of $Z=0.004$.

	Unbound	Primary WD	Primary NS	Primary BH
Unbound		0.0230	0.1681	0.0763
Secondary WD	0.0220	0.1175	0.0032	0.0048
Secondary NS	0.0897	0.00005	0.0002	0.0024
Secondary BH	0.0461	0.0010	0.0014	0.0214
Single		0.1279	0.1887	0.1063

Table 9. The mean space velocities of different single and binary compact remnants at a metallicity of $Z=0.004$.

	Unbound	Primary WD	Primary NS	Primary BH
Unbound		10 ± 2	420 ± 180	95 ± 72
Secondary WD	26 ± 20	0	81 ± 39	56 ± 30
Secondary NS	380 ± 180	89 ± 29	160 ± 65	97 ± 46
Secondary BH	93 ± 55	76 ± 36	87 ± 55	37 ± 28
Single		0	430 ± 180	94 ± 71

Salvaterra R., Devecchi B., Colpi M., D’Avanzo P., 2010, MNRAS, 727S

Schmidt-Kaler Th., 1982, in Landolt-Bornstein New Series, Group VI, vol. 2b, ed. K. Schaifers, & H. H. Voigt (Springer-Verlag), 1

van der Sluys M.V., Lamers H.J.G.L.M., 2003, A&A, 398, 181V

Smartt S.J., Eldridge J.J., Crockett R.M., Maund J.R., 2009, MNRAS in press

Stone R.C., 1991, AJ, 102, 333S

Tauris T.M., Takens R.J., 1998, A&A, 330, 1047T

Tauris T.M., Fender R.P., van den Heuvel E.P.J., Johnston H.M., Wu K., 1999, MNRAS, 310, 1165

Thompson T.A., Kistler M.D., Stanek K.Z., arXiv:0912.0009

Tout C.A., Aarseth S.J., Pols O.R., Eggleton P.P., 1997,

MNRAS, 291, 732T

Ueta et al. 2008, PASJ, 60, S407

Vanbeveren D., De Loore C., Van Rensbergen W., 1998, A&AR, 9, 63

Vanbeveren D., van Rensbergen W., De Loore C., 1998, ASSL, 232

Vanbeveren D., 2001, in *The influence of binaries on stellar population studies*, Dordrecht: Kluwer Academic Publishers, 2001, xix, 582 p. Astrophysics and space science library (ASSL), Vol. 264. ISBN 0792371046, p.249

Vanbeveren D., Van Bever J., Belkus H., 2007, astro-ph/0703796

van der Hucht K.A., 2001, NewAR, 45, 135V

van Kerkwijk M. H., Kulkarni S. R., 1999, ApJ, 516L, 25V
van Rensbergen W., Vanbeveren D., de Loore C., 1996, A&A, 305, 825

Table 10. The relative rates of the different SN types and their progenitors mean effective initial mass, mean space velocity and mean distance travelled from point of origin at a metallicity of $Z=0.020$. The relative rates and means are also split up into the values for single stars, primaries and secondaries.

		IIP	non-IIP	Ib	Ic	L-GRB
Fraction	All	0.582	0.119	0.068	0.231	0.0
	Single	0.287	0.046	0.007	0.058	0.0
	Primary	0.150	0.055	0.045	0.123	0.0
	Secondary	0.144	0.018	0.016	0.050	0.0
$\langle M_i \rangle$ [M_\odot]	All	10.7 ± 3.0	17.7 ± 6.3	16.8 ± 5.8	37.1 ± 22.8	
	Single	11.1 ± 2.9	21.9 ± 2.3	27.5 ± 0.5	50.7 ± 21.8	
	Primary	10.1 ± 2.9	13.2 ± 5.4	15.6 ± 4.5	32.7 ± 22.5	
	Secondary	10.5 ± 3.2	20.3 ± 6.6	15.6 ± 5.8	32.3 ± 18.0	
$\langle v_{\text{run}} \rangle$ [km s^{-1}]	All	4.4 ± 12.0	2.0 ± 6.1	5.0 ± 13.4	4.0 ± 10.8	
	Single	0.0	0.0	0.0	0.0	
	Primary	0.2 ± 1.2	1.0 ± 3.5	0.3 ± 1.8	0.4 ± 1.9	
	Secondary	17.5 ± 18.7	10.0 ± 11.6	20.3 ± 21.0	17.4 ± 17.4	
$\langle d_{\text{run}} \rangle$ [pc]	All	48 ± 210	10 ± 39	35 ± 150	17 ± 74	
	Single	0.0	0.0	0.0	0.0	
	Primary	2 ± 16	8 ± 36	2 ± 15	1 ± 10	
	Secondary	190 ± 380	38 ± 71	150 ± 280	74 ± 150	
$\langle t_{\text{run}} \rangle$ [Myr]	All	36 ± 31	22 ± 38	21 ± 21	9 ± 7	
	Single	26 ± 10	9 ± 1	7.0 ± 0.1	5 ± 1	
	Primary	33 ± 15	26 ± 20	17 ± 9	10 ± 5	
	Secondary	57 ± 52	46 ± 85	37 ± 34	13 ± 11	

Table 11. The relative rates of the different SN types and their progenitors mean effective initial mass, mean space velocity and mean distance travelled from point of origin at a metallicity of $Z=0.004$. The relative rates and means are also split up into the values for single stars, primaries and secondaries. The mean mass in brackets for the long-GRBs is the actual initial mass before the stars have accreted material from the primary.

		IIP	non-IIP	Ib	Ic	L-GRB
Fraction	All	0.605	0.141	0.164	0.091	0.001
	Single	0.324	0.055	0.025	0.000	0.0
	Primary	0.163	0.079	0.079	0.055	0.0
	Secondary	0.118	0.008	0.060	0.036	0.001
$\langle M_i \rangle$ [M_\odot]	All	9.9 ± 3.4	21.4 ± 10.0	30.0 ± 25.3	25.6 ± 18.5	$40.7 \pm 16.8(15.2 \pm 12.1)$
	Single	10.6 ± 3.5	28.4 ± 5.9	66.2 ± 20.4	–	
	Primary	9.2 ± 3.1	16.3 ± 9.5	28.5 ± 24.0	22.8 ± 17.9	
	Secondary	9.0 ± 2.8	24.4 ± 5.4	17.3 ± 11.1	30.0 ± 18.4	$40.7 \pm 16.8(15.2 \pm 12.1)$
$\langle v_{\text{run}} \rangle$ [km s^{-1}]	All	4.2 ± 12.1	1.0 ± 3.6	6.0 ± 14.0	8.6 ± 16.3	12.0 ± 10.9
	Single	0.0	0.0	0.0	–	
	Primary	0.1 ± 0.9	0.6 ± 2.1	0.3 ± 1.6	0.2 ± 1.2	
	Secondary	21.2 ± 19.9	12.7 ± 6.5	15.8 ± 19.4	21.3 ± 19.9	12.0 ± 10.9
$\langle d_{\text{run}} \rangle$ [pc]	All	54 ± 240	3 ± 19	75 ± 250	60 ± 150	88 ± 100
	Single	0.0	0.0	0.0	0.0	
	Primary	0.5 ± 4	3 ± 21	3 ± 21	1 ± 6	
	Secondary	280 ± 480	27 ± 35	200 ± 390	150 ± 210	88 ± 100
$\langle t_{\text{run}} \rangle$ [Myr]	All	39 ± 25	15 ± 12	27 ± 30	16 ± 7	15 ± 5
	Single	31 ± 14	8 ± 1	4 ± 1	–	
	Primary	41 ± 20	21 ± 14	17 ± 15	15 ± 7	
	Secondary	58 ± 40	9 ± 2	49 ± 36	17 ± 7	15 ± 5

- Vink J.S., de Koter A., Lamers H.J.G.L.M., 2001, *A&A*, 369, 574
Voss R., Tauris T.M., 2003, *MNRAS*, 342, 1169V
Wellstein S., Langer N., 1999, *A&A*, 350, 148
Woosley S.E., Bloom J.S., 2006, *ARA&A*, 44, 507
Yoon S.-C., Langer N., 2005, *A&A*, 443, 643Y
Yoon S.-C., Langer N., Norman C., 2006, *A&A*, 460, 199Y
Yoon S.-C., Woosley S.E., Langer N., 2010, arXiv1004.0843Y
Zinnecker H., Yorke H.W., 2007, *ARA&A*, 45, 481Z

6 APPENDIX

In this appendix, we present additional results from our simulations. These are placed here not to divert the main results we wished to cover. These Figures contain similar information to that presented in the main paper. However these provide greater clarity on some specific results of the simulation. Fig. 12 is similar to Fig. 3 but with the range of velocities included widened to cover velocities less than those typically expected for runaway stars. Fig. 13 is similar to Fig. 9 but is over a linear distance scale. Fig. 14 is also similar to Fig. 9 but is for cumulative probability. Then Figs. 15 and 16 are also similar to these plots but split the SN events up into different initial-mass ranges rather than SN types. Finally Figs. 17 are similar to the other plots but show results for the compact-object mergers rather than SNe.

This paper has been typeset from a $\text{\TeX}/\text{\LaTeX}$ file prepared by the author.

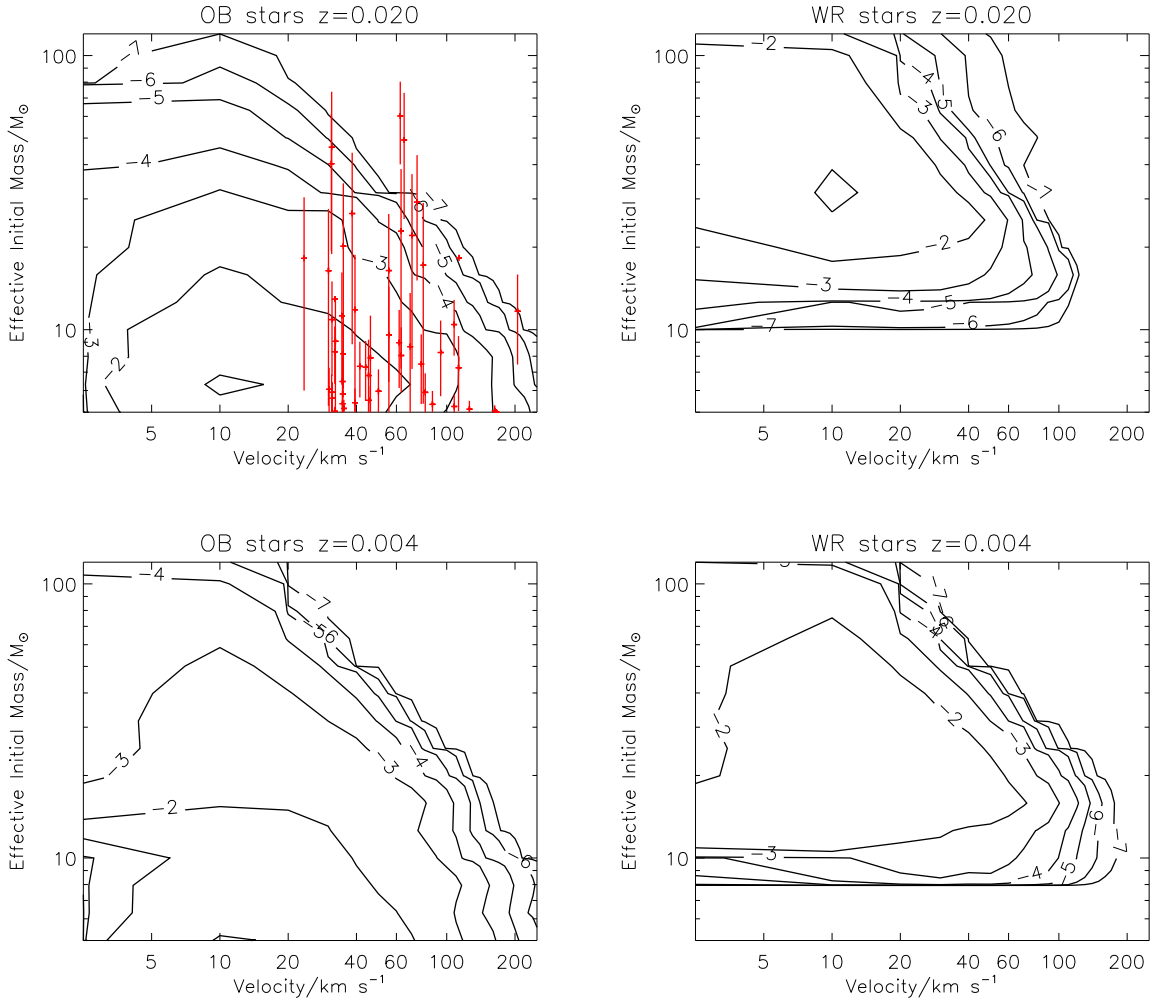


Figure 12. Similar to Figure 3 but with the velocity range below the normal velocity limit required for a star to be identified as a runaway.

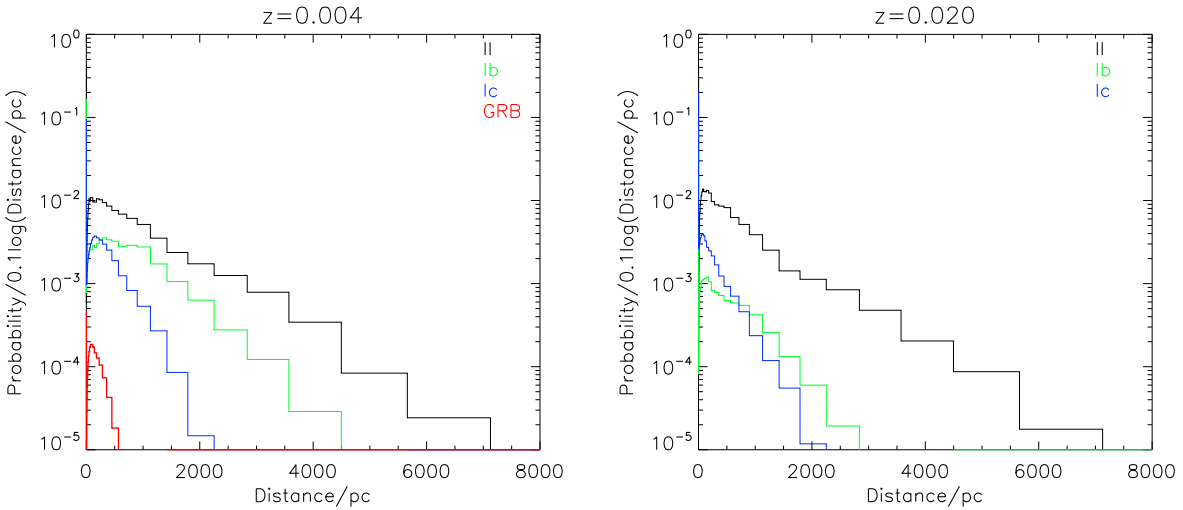


Figure 13. Similar to the upper left panels in Figures 9 and 10 but with a linear scale on the x-axis.

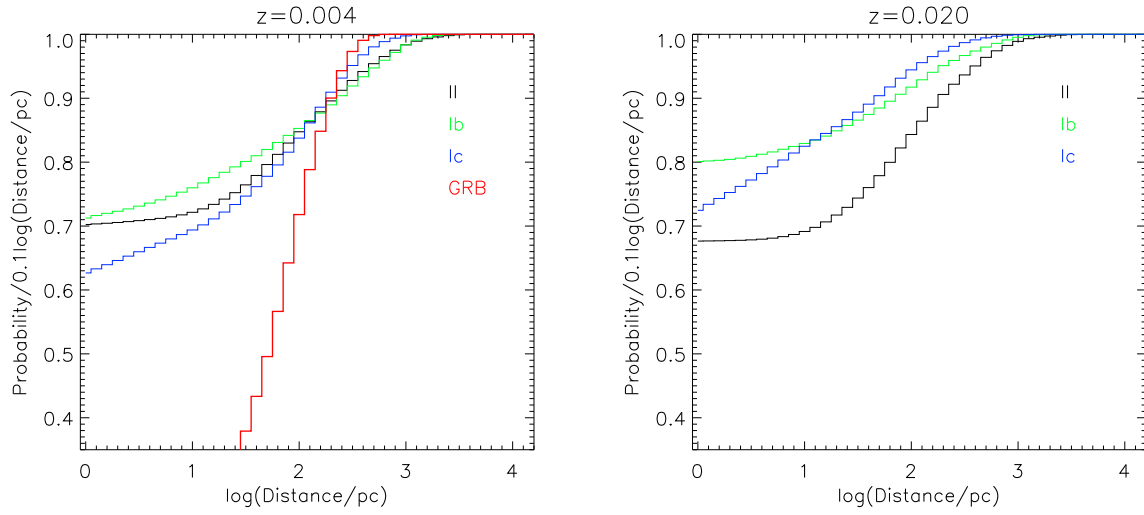


Figure 14. Similar to the upper left panels in Figures 9 and 10 but with the cumulative probability with increasing progenitor distance on the y-axis with a linear scale.

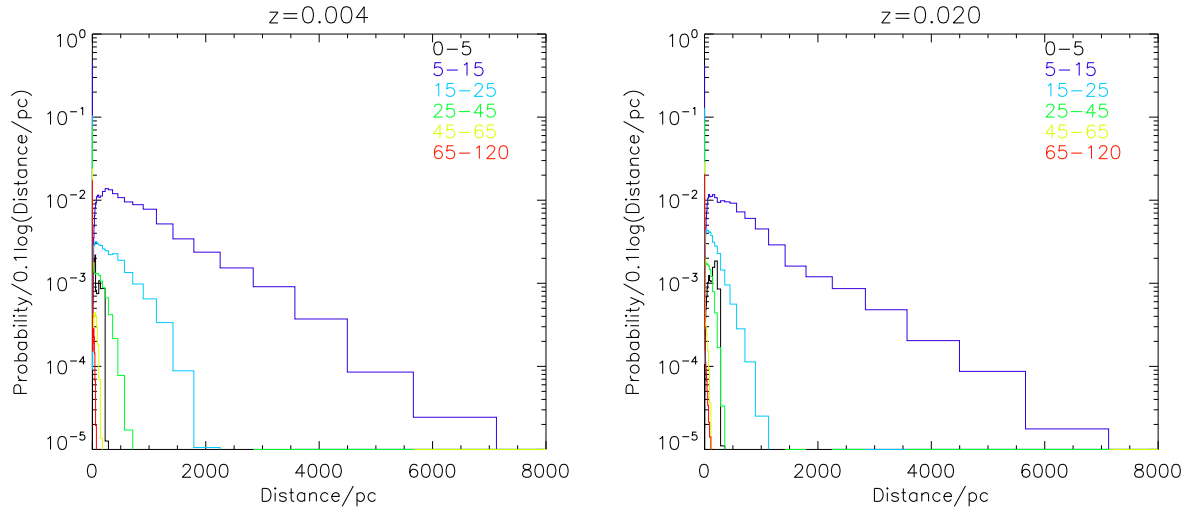


Figure 15. Similar to the upper left panels in Figures 9 and 10 but with a linear scale on the x-axis and the lines now represent different initial mass ranges for the progenitor stars.

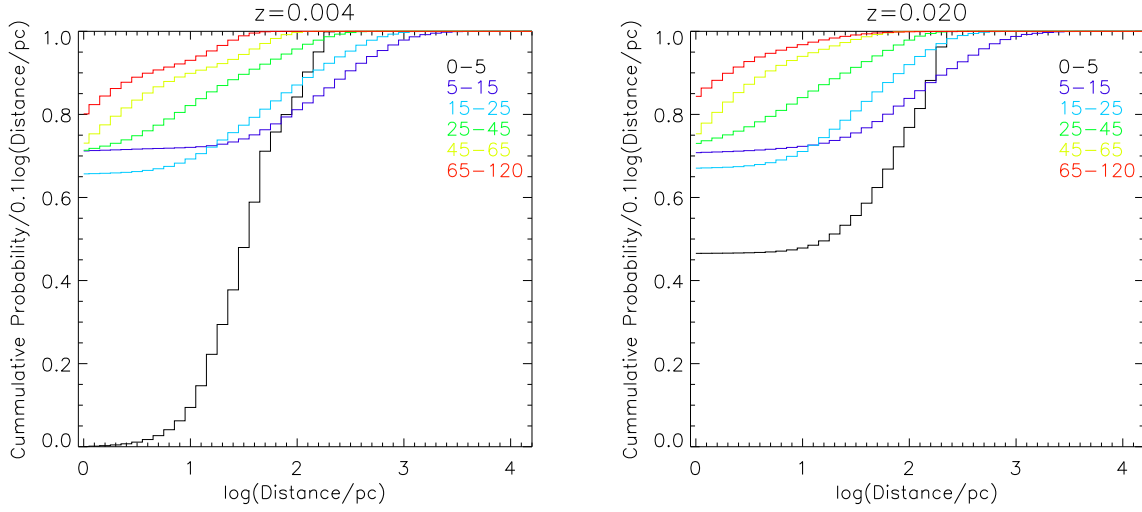


Figure 16. Similar to the upper left panels in Figures 9 and 10 with the cumulative probability with increasing progenitor distance on the y-axis with a linear scale with a linear scale.

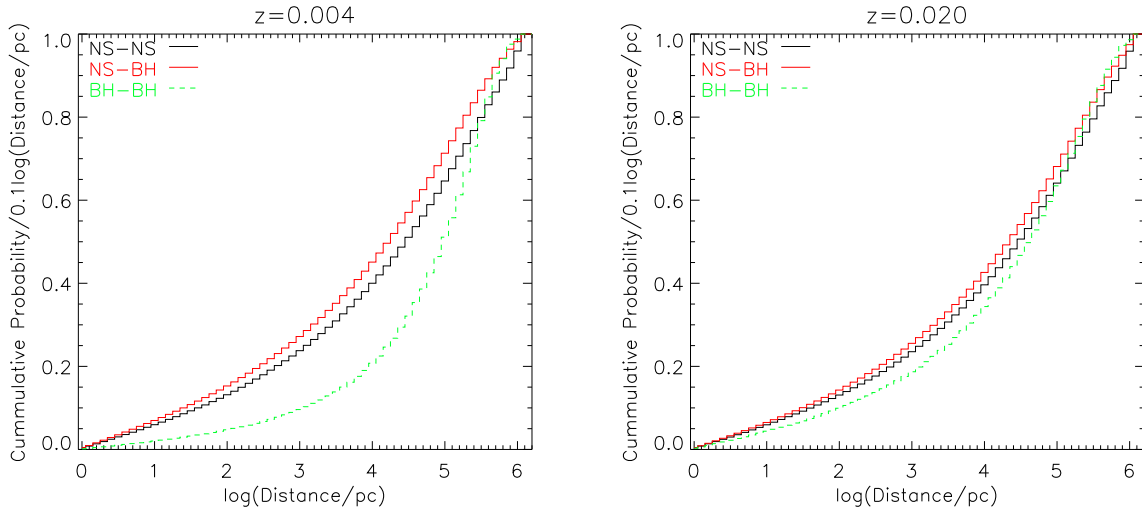


Figure 17. Similar to the upper left panels in Figures 9 but now for the mergers of compact objects shown in Figure 11 with the cumulative probability of a merger versus increasing progenitor distance on the y-axis with a linear scale with a linear scale.